



# Genetic Diversity of Collaborative Cross Mice Controls Viral Replication, Clinical Severity, and Brain Pathology Induced by Zika Virus Infection, Independently of *Oas1b*

Caroline Manet,<sup>a</sup> Etienne Simon-Lorière,<sup>b</sup> Grégory Jouvion,<sup>c,d</sup> David Hardy,<sup>d</sup> Matthieu Prot,<sup>b</sup> Laurine Conquet,<sup>a</sup> Marie Flamand,<sup>e</sup> Jean-Jacques Panthier,<sup>a</sup> Anavaj Sakuntabhai,<sup>f</sup> Xavier Montagutelli<sup>a</sup>

<sup>a</sup>Mouse Genetics Laboratory, Department of Genomes and Genetics, Institut Pasteur, Paris, France

<sup>b</sup>Evolutionary Genomics of RNA Viruses, Department of Virology, Institut Pasteur, Paris, France

<sup>c</sup>Sorbonne Université, INSERM, Pathophysiology of Pediatric Genetic Diseases, AP-HP, Hôpital Armand-Trousseau, UF de Génétique Moléculaire, Paris, France

<sup>d</sup>Institut Pasteur, Experimental Neuropathology Unit, Department of Global Health, Paris, France

<sup>e</sup>Structural Virology Unit, Department of Virology, CNRS UMR 3569, Institut Pasteur, Paris, France

<sup>f</sup>Functional Genetics of Infectious Diseases Unit, Department of Global Health, CNRS UMR 2000, Institut Pasteur, Paris, France

**ABSTRACT** The explosive spread of Zika virus (ZIKV) has been associated with major variations in severe disease and congenital afflictions among infected populations, suggesting an influence of host genes. We investigated how genome-wide variants could impact susceptibility to ZIKV infection in mice. We first describe that the susceptibility of *Ifnar1*-knockout mice is largely influenced by their genetic background. We then show that Collaborative Cross (CC) mice, which exhibit a broad genetic diversity, in which the type I interferon receptor (IFNAR) was blocked by an anti-IFNAR antibody expressed phenotypes ranging from complete resistance to severe symptoms and death, with large variations in the peak and the rate of decrease in the plasma viral load, in the brain viral load, in brain histopathology, and in the viral replication rate in infected cells. The differences in susceptibility to ZIKV between CC strains correlated with the differences in susceptibility to dengue and West Nile viruses between the strains. We identified highly susceptible and resistant mouse strains as new models to investigate the mechanisms of human ZIKV disease and other flavivirus infections. Genetic analyses revealed that phenotypic variations are driven by multiple genes with small effects, reflecting the complexity of ZIKV disease susceptibility in the human population. Notably, our results rule out the possibility of a role of the *Oas1b* gene in the susceptibility to ZIKV. Altogether, the findings of this study emphasize the role of host genes in the pathogeny of ZIKV infection and lay the foundation for further genetic and mechanistic studies.

**IMPORTANCE** In recent outbreaks, ZIKV has infected millions of people and induced rare but potentially severe complications, including Guillain-Barré syndrome and encephalitis in adults. While several viral sequence variants were proposed to enhance the pathogenicity of ZIKV, the influence of host genetic variants in mediating the clinical heterogeneity remains mostly unexplored. We addressed this question using a mouse panel which models the genetic diversity of the human population and a ZIKV strain from a recent clinical isolate. Through a combination of *in vitro* and *in vivo* approaches, we demonstrate that multiple host genetic variants determine viral replication in infected cells and the clinical severity, the kinetics of blood viral load, and brain pathology in mice. We describe new mouse models expressing high degrees of susceptibility or resistance to ZIKV and to other flaviviruses. These models will facilitate the identification and mechanistic characterization of host genes that influence ZIKV pathogenesis.

**KEYWORDS** Zika virus, flavivirus, mouse model, host genetics, genetic diversity, Collaborative Cross, Zika

**Citation** Manet C, Simon-Lorière E, Jouvion G, Hardy D, Prot M, Conquet L, Flamand M, Panthier J-J, Sakuntabhai A, Montagutelli X. 2020. Genetic diversity of Collaborative Cross mice controls viral replication, clinical severity, and brain pathology induced by Zika virus infection, independently of *Oas1b*. *J Virol* 94:e01034-19. <https://doi.org/10.1128/JVI.01034-19>.

**Editor** Adolfo García-Sastre, Icahn School of Medicine at Mount Sinai

**Copyright** © 2020 American Society for Microbiology. All Rights Reserved.

Address correspondence to Xavier Montagutelli, [xavier.montagutelli@pasteur.fr](mailto:xavier.montagutelli@pasteur.fr).

**Received** 19 June 2019

**Accepted** 3 November 2019

**Accepted manuscript posted online** 6 November 2019

**Published** 17 January 2020

Zika virus (ZIKV) is a mosquito-borne flavivirus isolated in 1947 from a febrile rhesus monkey in Uganda (1). Until 2007, ZIKV had circulated in Africa and Asia, causing mild flu-like syndromes, with rare reported clinical cases (2). However, during recent epidemics, ZIKV infection triggered severe complications, including Guillain-Barré syndrome and encephalitis in adults (3, 4) and congenital malformations in the fetuses of infected pregnant women (5, 6). Viral mutations may have contributed to the enhanced pathogenicity of ZIKV (7, 8) but only partly explain the variable proportion of symptomatic infections between populations (9) and the increased incidence of congenital Zika syndrome (CZS) in Polynesia (10) and Brazil (11), suggesting a role for host genetic variants. Recent evidence indicates that the regulation of innate immunity genes is driven by the host genetic background in human fetal brain-derived neural stem cells (hNSCs) infected *in vitro* with ZIKV (12). Additionally, the analysis of pairs of dizygotic twins exposed to ZIKV during pregnancy and discordant for CZS suggests multigenic host susceptibility to ZIKV-induced brain malformations (13).

Multiple mouse models have been proposed to decipher the mechanisms of ZIKV disease pathogenesis (14, 15). These models allow the investigation of several key features of human infection, such as neuronal damage (16, 17), sexual and vertical transmission (18–21), and fetal demise and CZS (22–25). However, while nonstructural ZIKV proteins efficiently inhibit the innate antiviral responses in humans (26, 27), allowing viral replication, ZIKV replicates poorly in wild-type mice due to the inability of its NS5 protein to antagonize the STAT2 protein and the type I interferon (IFN) response as it does in humans (28). Effective systemic infection in mice occurs when this response is abrogated by genetically inactivating the *Irfar1* gene (29) or by blocking the type I IFN receptor (IFNAR) with the MAR1-5A3 monoclonal antibody (MAb) (30, 31). So far, the host genetic factors involved in mouse susceptibility to ZIKV infection have been investigated mainly through reverse genetic approaches, by studying the consequences of genetic ablation of specific genes, such as innate or adaptive immunity genes (29, 32–35). While these models have contributed to our understanding of the mechanisms of ZIKV disease, they do not model the simultaneous contribution of variants in multiple pathways like those that would most likely be observed in the natural population. A recent study has reported strain-specific differences in susceptibility to neonatal ZIKV infection across four mouse laboratory strains, affecting neuropathology and behavior in adulthood (36). More extensive studies investigating the role of genome-wide genetic variations on susceptibility to ZIKV infection, using mouse models that reflect the phenotypic and genetic diversity of the human population, are needed (37).

In this study, we addressed this question using two types of susceptible mouse models. First, since the phenotype resulting from a single gene modification often varies under the influence of modifier genes (38, 39), we assessed the effect of host genetic background on the susceptibility of *Irfar1*-deficient mice. We then investigated the impact of host genetic diversity on the susceptibility to ZIKV infection in the Collaborative Cross (CC), a panel of recombinant inbred mice produced via a funnel breeding scheme that combined eight founder inbred strains, including five classic laboratory strains and three wild-derived strains (40). As a result, every CC strain has inherited a unique and balanced contribution from each of the eight founder strains. These founder strains capture approximately 90% of the genetic variants present in the *Mus musculus* species (41), and the resulting CC strains, which segregate an estimated 45 million polymorphisms, have more genetic diversity than the human population (42). Extensive variations in pathogenic phenotypes have been previously reported in the CC panel after viral (43–50), bacterial (51, 52), and fungal (53) infections, demonstrating that this resource is ideally suited for investigating the role of host genetic variants in the pathophysiology of infectious diseases (54).

Susceptibility to ZIKV in *Irfar1*-deficient mice was strongly influenced by the genetic background, which has practical implications for future virology studies to identify modifier genes. The challenge of 35 immunocompetent CC strains with ZIKV after MAR1-5A3 MAb treatment allowed efficient viral replication. We show that the genetic

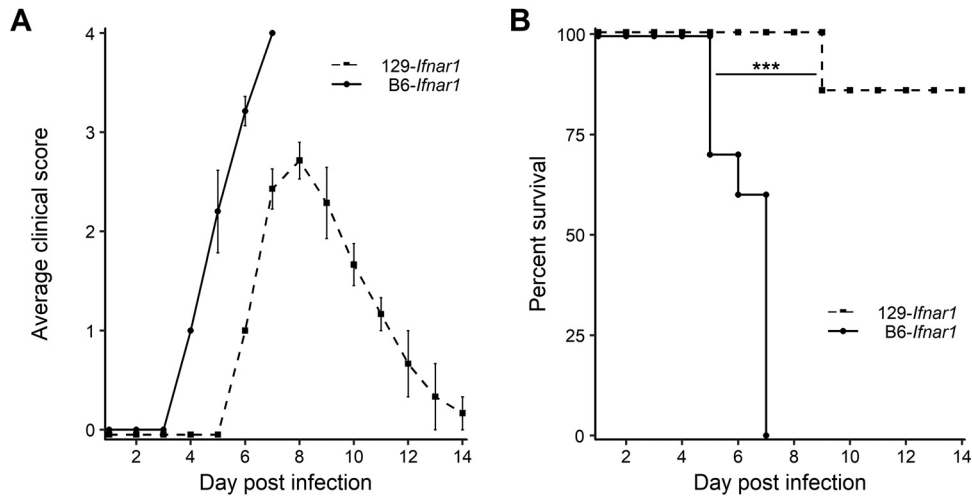


**FIG 1** ZIKV disease severity in *Ifnar1*-deficient mice is driven by the genetic background. Six- to 7-week-old 129-*Ifnar1* ( $n = 7$ ) and B6-*Ifnar1* ( $n = 10$ ) mice were infected i.p. with  $10^7$  FFUs of ZIKV FG15 and monitored for 14 days. (A) Average clinical score, with numerical values given as follows: 0, no symptoms; 1, ruffled fur; 2, emaciation, hunched posture, and/or hypoactivity; 3, hind limb weakness, prostration, and/or closed eyes; and 4, moribund or dead. (B) Kaplan-Meier survival curves showing 100% lethality in B6-*Ifnar1* mice at day 7 p.i. and the survival of 6/7 129-*Ifnar1* mice, \*\*\*,  $P = 0.0002$  (log-rank test). B6-*Ifnar1* mice developed early symptoms, which rapidly evolved to death, while 129-*Ifnar1* mice developed symptoms 2 days later, which eventually resolved in most mice.

diversity in the CC panel enabled large variations in the clinical severity of ZIKV disease, in the peak and the kinetics of the plasma viral load, and in the severity of ZIKV-induced brain pathology. The genetic diversity also resulted in differences in the permissiveness of CC mouse cells to viral replication, and these differences likely contribute to the *in vivo* phenotypic range. We found that the differences in the susceptibility of a subset of CC strains to ZIKV correlated with the differences in the susceptibility of the strains to dengue virus (DENV) and West Nile virus (WNV), suggesting shared underlying mechanisms. We identified highly susceptible and resistant mouse strains as new models to investigate the mechanisms of human ZIKV disease and other flavivirus infections. Finally, genetic analysis revealed that the susceptibility to ZIKV in the CC is driven by multiple loci with small individual effects and that *Oas1b*, a major determinant of mouse susceptibility to WNV, is not involved.

(This article was submitted to an online preprint archive [55].)

## RESULTS

### Genetic background controls the susceptibility of *Ifnar1*-deficient mice to ZIKV.

Many studies have used *Ifnar1*-knockout mice on the 129S2/SvPas mouse (here abbreviated 129 mouse) (56, 57) or C57BL/6J mouse (here abbreviated B6 mouse) (23, 29, 34) inbred background, but the differences in ZIKV susceptibility between these two strains have not been reported and remain unclear due to heterogeneous experimental conditions between studies. We compared the susceptibility of age-matched 129S2/SvPas *Ifnar1*<sup>-/-</sup> (129-*Ifnar1*) and C57BL/6J *Ifnar1*<sup>-/-</sup> (B6-*Ifnar1*) mice infected intraperitoneally (i.p.) with  $10^7$  focus-forming units (FFUs) of ZIKV FG15. B6-*Ifnar1* mice showed increasingly severe symptoms, with body weight loss, ruffled fur, ataxia, and hind limb paralysis from day 4 postinfection (p.i.), and all (10/10) B6-*Ifnar1* mice were moribund or dead by day 7 p.i. In contrast, 129-*Ifnar1* mice developed mild symptoms (ruffled fur, hunched back) starting on day 6 p.i. and declining over the second week of infection, with one mouse dying on day 9 p.i. (Fig. 1), demonstrating that the susceptibility to ZIKV infection conferred by *Ifnar1* genetic inactivation is critically influenced by the host genetic background.







### MAb blockade of IFNAR is a robust model to study ZIKV infection in CC mice.

*Ifnar1* genetic deficiency permanently abrogates alpha/beta IFN (IFN- $\alpha/\beta$ )-mediated

**TABLE 1** Origin of *Oas1b* and *Ifnar1* alleles in the 35 CC strains tested<sup>a</sup>

Strain	<i>Oas1b</i>	<i>Ifnar1</i>
CC001	B	F
CC002	A	B
CC003	H	B
CC004	G	B
CC005	B	E
CC006	E	D
CC007	D	B
CC009	E	D
CC011	B	G
CC012	H	A
CC013	E	E
CC017	H	D
CC018	D	C
CC019	H	C
CC021	C	D
CC024	E	A
CC025	H	A
CC026	A	H
CC027	B	G
CC032	B C *	B
CC037	B	C
CC039	H	B
CC040	B D *	D
CC041	F	D
CC042	H	F
CC043	C	C
CC045	C	H
CC049	B D *	D
CC051	E	B
CC059	E	B
CC060	D	F
CC061	E	A
CC068	B	E G *
CC071	C	F
CC072	C	D

functional			A/J allele
not functional			B6 allele or identical
			CAST allele
			PWK allele

<sup>a</sup>Data are from <http://csbio.unc.edu/CCstatus/CCGenomes/#genotypes>.  
 \*, heterozygous strain; A, A/J mice; B, C57BL/6J mice; C, 129S1/SvImJ mice; D, NOD/ShiLtJ mice; E, NZO/HiLtJ mice; F, CAST/EiJ mice; G, PWK/PhJ mice; H, WSB/EiJ mice.

immune responses but is not currently available on diverse genetic backgrounds. We therefore tested the suitability of transient IFNAR blockade mediated by MAb treatment as a model to study ZIKV infection in genetically diverse mice, like the CC mice. Since the MAR1-5A3 MAb was generated in a laboratory strain (the 129-*Ifnar1* mouse) (30) and since the CC strains differ in their *Ifnar1* allele (Table 1), we first compared the coding sequence of the *Ifnar1* gene across the eight founder strains. While 129S1/SvImJ, NOD/ShiLtJ, NZO/HiLtJ, and WSB/EiJ mice carry the same *Ifnar1* allele as C57BL/6J mice, the *Ifnar1* alleles of A/J, PWK/PhJ, and CAST/EiJ mice differ by 1, 3, and 7 amino acids from the C57BL/6J mouse reference sequence, respectively (Table 2). Notably, all three PWK/PhJ variants were found in CAST/EiJ mice. Therefore, we assessed the efficacy of the MAR1-5A3 MAb by Western blot analysis on mouse embryonic fibroblasts (MEFs) isolated from two CC strains (strains CC001 and CC071),

**TABLE 2** Variants in the coding sequence of the *Ifnar1* gene

Position <sup>a</sup>	dbSNP <sup>b</sup> annotation	Nucleotide in the <i>Ifnar1</i> gene of the CC founder strains:									Amino acid position	Amino acid change <sup>c</sup>
		Reference (B6)	129S1/SvlmJ	A/J	CAST/EiJ	NOD/ShiLtJ	NZO/HILtJ	PWK/PhJ	WSB/EiJ			
91,485,366	rs235809125	C	— <sup>d</sup>	—	T	—	—	—	—	—	8	A → V
91,485,368	rs255866699	G	—	—	A	—	—	—	—	—	9	A → T
91,499,433	rs31418313	G	—	A	—	—	—	—	—	—	274	R → H
91,499,468	rs223171563	A	—	—	G	—	—	—	—	—	286	N → D
91,499,532	rs240163845	A	—	—	G	—	—	G	—	—	307	H → R
91,501,623	rs263194450	T	—	—	G	—	—	G	—	—	376	I → R
91,501,631	rs246470801	G	—	—	A	—	—	A	—	—	379	E → K
91,505,284	rs219805193	C	—	—	T	—	—	—	—	—	549	A → V

<sup>a</sup>The sequences at positions 91,485,344 to 91,505,411 on chromosome 16 were retrieved from the Sanger Institute Mouse Genomes Project ([https://www.sanger.ac.uk/sanger/Mouse\\_SnpViewer/rel-1505](https://www.sanger.ac.uk/sanger/Mouse_SnpViewer/rel-1505)).

<sup>b</sup>dbSNP, Single Nucleotide Polymorphism Database.

<sup>c</sup>Amino acid changes compared with the reference (B6 mouse) sequence (CCDS database; <https://www.ncbi.nlm.nih.gov/CCDS/>).

<sup>d</sup>—, no nucleotide change.

both of which inherited the *Ifnar1* allele from the most divergent CAST/EiJ strain (58), by comparison with that on B6 MEFs. IFNAR stimulation by IFN- $\alpha/\beta$  activates the JAK1/TYK2 pathway and results in the phosphorylation of STAT1. We found that in B6, CC001, and CC071 MEFs, STAT1 phosphorylation was equally induced by murine IFN- $\alpha$  and fully inhibited by the MAR1-5A3 MAb (Fig. 2A).

To assess MAR1-5A3 MAb efficacy *in vivo*, we infected the CC001 and CC071 strains with  $10^7$  FFUs of ZIKV FG15 i.p. and we measured the kinetics of the plasma viral load in mice with and without 2 mg MAb treatment 24 h prior to infection. Consistent with previous studies in B6 (31, 59) and BALB/c (60) mice, the viral load was consistently 4 to 5  $\log_{10}$  units higher in MAb-treated mice of both the CC001 and CC071 strains than in untreated mice, demonstrating that MAR1-5A3 MAb treatment successfully increases CC mouse permissiveness to ZIKV replication (Fig. 2B).

We then measured the kinetics of the plasma viral load in the 129-*Ifnar1* strain as well as in four MAb-treated CC strains infected with  $10^7$  FFUs of ZIKV FG15 i.p. We established that the peak plasma viral load occurred in most individuals at day 2 p.i., independently of the mouse genetic background (Fig. 2C).

In previous studies, viral loads have been measured either by FFU titration or by reverse transcription (RT)-quantitative PCR (qPCR) quantification of viral genome copies. We compared these two methods in the B6-*Ifnar1* and 129-*Ifnar1* strains and in 10 MAb-treated CC strains (Fig. 2D). We performed focus-forming assays (FFA) to measure the viral particles in the plasma at day 2 p.i. and confirmed the production of infectious ZIKV in the blood of all strains. Next, we compared the plasma viral load measured by RT-qPCR and by FFA. We found that these two parameters were strongly correlated over a 2- $\log_{10}$  range (Pearson's coefficient [ $r^2$ ] = 0.89,  $P = 9.9 \times 10^{-17}$ ), with the number of genome copies being, on average, 3  $\log_{10}$  units higher than the number of FFUs (Fig. 2D). We therefore validated that the plasma viral load measured by RT-qPCR, a more labor-efficient method, could be used as a proxy for viremia throughout the study.

Finally, we compared the plasma viral loads at day 2 p.i. between male and female 129-*Ifnar1* mice and both sexes of 4 MAb-treated CC strains that had been tested. We found no significant difference between sexes across diverse genetic backgrounds (two-way analysis of variance [ANOVA],  $P = 0.24$ ) (Fig. 2E), validating the use of merged data from males and females in mouse ZIKV infection experiments.

**CC genetic diversity drives ZIKV disease severity and plasma viral load.** To explore broad genetic variation, we assessed the susceptibility of MAb-treated mice of 35 CC strains. B6-*Ifnar1*, 129-*Ifnar1* and MAb-treated B6 mice were included as reference strains. Among non-*Ifnar1*-deficient mice, only mice of three CC strains developed symptoms, as shown in Fig. 3A, which summarizes the clinical observations made at day 7 p.i. CC021 and CC026 mice recovered and survived, while symptoms worsened in 7/9 (78%) CC071 mice, which were moribund or died between days 7 and 9 p.i.

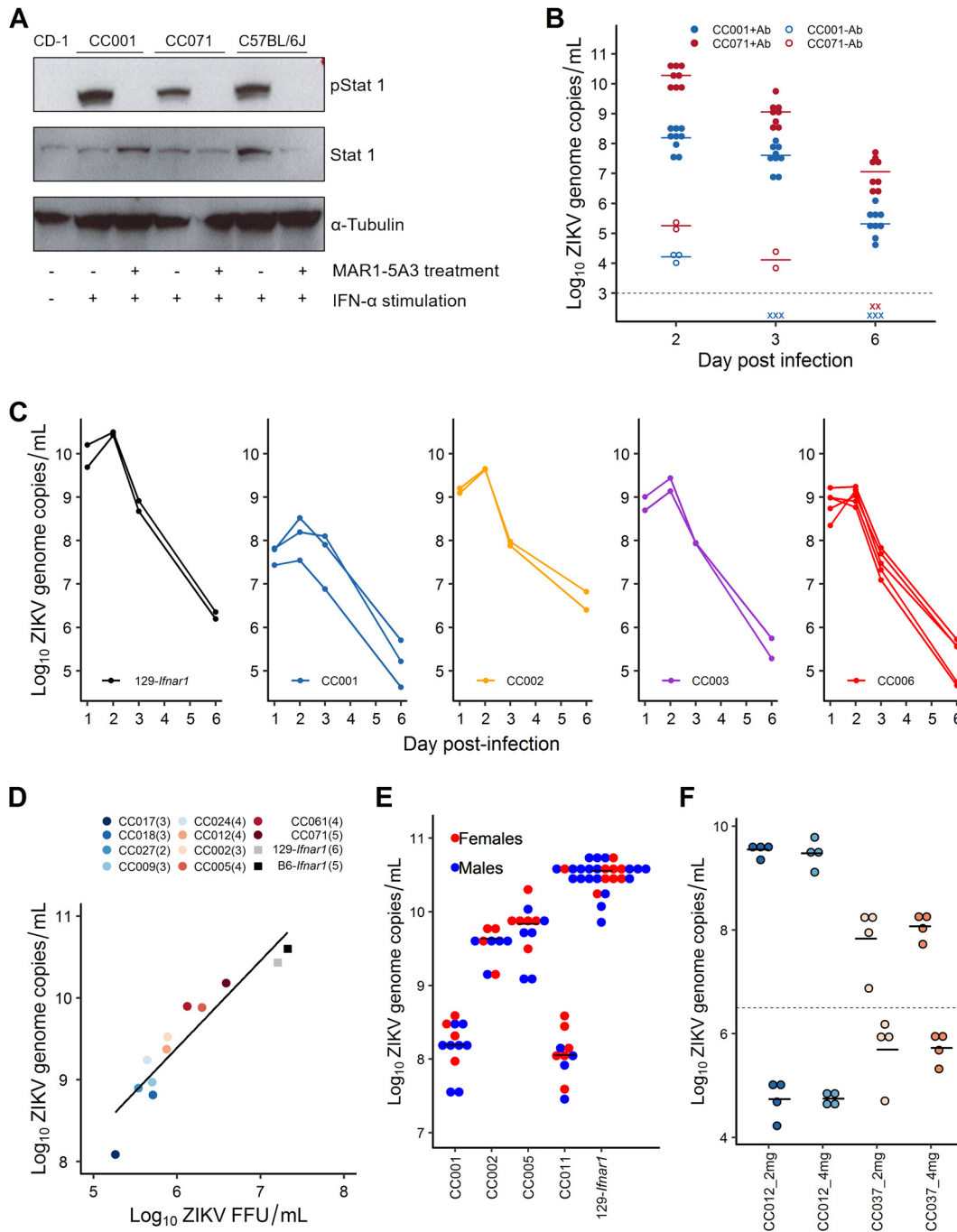


**FIG 2** Establishment and validation of the experimental conditions for assessing susceptibility to ZIKV in CC strains. (A) The efficacy of the MAR1-5A3 MAb (100  $\mu$ g for  $5 \times 10^6$  cells) at blocking the IFNAR receptor in diverse mouse genetic backgrounds was determined by assessing STAT1 phosphorylation (pStat 1) by Western blotting on mouse embryonic fibroblasts (MEFs) derived from the C57BL/6J, CC001, CC071, and CD-1 strains. (B) Plasma viral load, measured on days 2, 3, and 6 p.i. by RT-qPCR, in 6- to 8-week-old mice of the CC001 and CC071 strains that had been treated with MAb MAR1-5A3 24 h prior to ZIKV infection (filled circles;  $n = 9$  and  $8$ , respectively) or untreated (open circles;  $n = 3$  and  $2$ , respectively).  $x$ , a sample with a level below the detection level. (C) Kinetics of the plasma viral load in 129-*Ilfnar1* mice and 4 CC strains measured by RT-qPCR. Each circle represents the result for a 6- to 8-week-old mouse analyzed on days 1, 2, 3, and 6. (D) Correlation between the plasma viral load determined by FFA ( $x$  axis) and RT-qPCR ( $y$  axis) in 46 blood samples from 129-*Ilfnar1* and B6-*Ilfnar1* mice and 10 CC strains (circles show the mean for each strain; the number of 6- to 8-week-old mice per strain is shown in parentheses). (E) Plasma viral load, measured by RT-qPCR at day 2 p.i., in 6- to 8-week-old males and females of the 129-*Ilfnar1* strain and of 4 CC strains ( $n \geq 4$  mice per group). (F) Effect of the dose of MAR1-5A3 antibody treatment on the rate of decrease of the plasma viral load. Seven- to 9-week-old mice of the CC012 and CC037 strains (4 mice per group) received 2 mg of the MAR1-5A3 MAb 1 day prior to being inoculated i.p. with  $10^7$  FFUs of ZIKV FG15. The groups receiving 4 mg of the MAb received additional i.p. injections of 1 mg of MAb on days 2 and 4 p.i. The plasma viral load was measured on days 2 and 6 p.i. (and the results are presented above and below the dashed line, respectively).

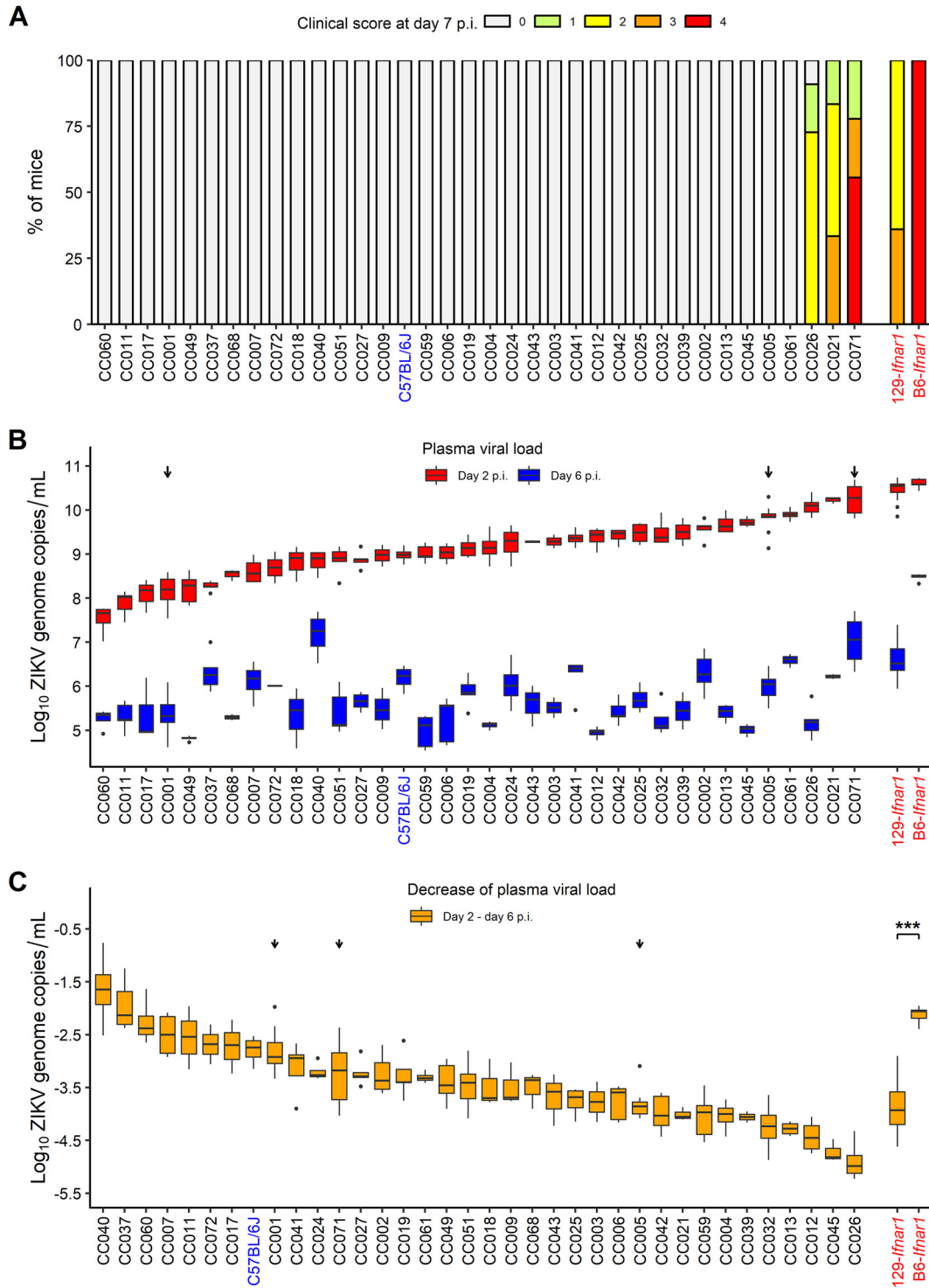


**FIG 3** CC genetic diversity strongly impacts the clinical severity of infection and the plasma viral load. Thirty-five CC strains ( $n = 2$  to 9 6- to 8-week-old mice per strain) were infected i.p. with  $10^7$  FFUs of ZIKV FG15 at 24 h after i.p. injection of 2 mg of the MAR1-5A3 MAbs. 129-Irfnar1 ( $n = 24$ ) and B6-Irfnar1 ( $n = 5$ ) mice were similarly infected without MAb treatment. (A) Clinical scores at day 7 p.i. as the percentage of mice in the five levels of severity (as described in the legend to Fig. 1). (B) Plasma viral load at days 2 p.i. (upper values) and 6 p.i. (lower values) quantified by RT-qPCR, shown as box-whisker plots, with outliers shown as dots (the strains are shown in the same order in which they are shown in panel A). (C) Difference between plasma viral loads at days 2 and 6 p.i. Strains are sorted by increasing absolute difference and are therefore in an order different from that in panels A and B. (B and C) Arrows indicate the subset of CC mouse strains selected for detailed study.

The plasma viral load was measured on days 2 and 6 p.i. At day 2 p.i., which corresponded to the time of peak viral load, the viral load was generally characterized by small within-strain heterogeneity and large interstrain variations spread over a  $2.8\text{-log}_{10}$  range (Fig. 3B), demonstrating a strong effect of host genes (Kruskal-Wallis test,  $P = 4.8 \times 10^{-15}$ ) with a broad-sense heritability of 86% (61). The three symptomatic CC strains showed the highest peak viral load, close to that of B6-*Ifnar1* and 129-*Ifnar1* mice. However, other strains (such as CC005 and CC061) had similarly high viral loads but never showed any clinical signs of disease, indicating that the peak viral load is unlikely the sole factor controlling clinical severity. At day 6 p.i., within-strain variations were larger and more heterogeneous, but we still observed highly significant interstrain differences (Kruskal-Wallis test,  $P = 1.1 \times 10^{-10}$ ). Interestingly, the viral loads on days 2 and 6 p.i. were only moderately correlated (Pearson's coefficient [ $r^2$ ] = 0.46;  $P = 0.004$ ), indicating that the viral load at day 2 p.i. was not predictive of the viral load at day 6 p.i. (see, for example, the results for CC018 and CC040 mice or CC026 and CC071 mice in Fig. 3B).

We used the difference in the  $\log_{10}$  plasma viral loads between days 2 and 6 p.i. to estimate the clearance rate of the virus from the bloodstream (Fig. 3C, in which the order of the strains sorted by increasing clearance rate was therefore different from that in Fig. 3A and B). This rate varied over a  $3.3\text{-log}_{10}$  range between strains, demonstrating a strong effect of host genes (Kruskal-Wallis test,  $P = 2.2 \times 10^{-12}$ ) with a broad-sense heritability of 76%. B6-*Ifnar1* mice showed a slower decrease in the viral load than 129-*Ifnar1* mice (Wilcoxon rank-sum test,  $P = 1.7 \times 10^{-5}$ ), despite similar peak viral loads at day 2 p.i. To confirm that the differences between CC strains were not due to differential rates of MAR1-5A3 antibody turnover, we treated CC012 mice (which showed a 4.4-log decrease) and CC037 mice (which showed a 1.9-log decrease) with 2 mg of MAb 24 h before ZIKV infection and then treated or did not treat them with two additional injections of 1 mg of MAb on days 2 and 4 postinfection. No differences in plasma viral load on days 2 and 6 p.i. were observed between the two conditions (Fig. 2F).

Overall, the genetic diversity in the CC panel controlled the clinical severity of the ZIKV infection, mouse survival, the peak plasma viral load, and the clearance rate of the plasma viral load. Of note, there was no association, across the 35 CC strains tested, between the peak plasma viral load and the *Ifnar1* allele inherited from the founder strain (ANOVA,  $P > 0.09$ ). The findings from this analysis confirm our *in vitro* data (Fig. 2A) and indicate that the variations in peak plasma viral load do not result from differences in MAb treatment efficacy due to MAb turnover or due to the *Ifnar1* alleles.

From this screening, we identified several strains with extreme phenotypes, in particular, strain CC071, which was the most susceptible to ZIKV infection; strains CC001, CC011, CC017, and CC060, which had low peak plasma viral loads; strain CC040, which had a slowly decreasing plasma viral load; and strains CC045 or CC026, which had high peak plasma viral loads but fast-decreasing plasma viral loads.

**CC mice show correlated susceptibility to ZIKV, DENV, and WNV.** We further characterized three CC strains (indicated by arrows in Fig. 3B and C) among those showing the lowest peak viral loads (strain CC001) and the highest peak viral loads with (strain CC071) or without (strain CC005) clinical symptoms. To establish whether the above-described differences were specific to the FG15 ZIKV strain of the Asian lineage, we first assessed the susceptibilities of the three selected strains to the HD78788 ZIKV strain of the African lineage. 129-*Ifnar1* mice and MAb-treated CC mice were infected i.p. with  $10^3$  FFUs of ZIKV HD78788, which proved to be highly pathogenic in *Ifnar1*-deficient mice, with rapid and severe symptoms and 100% mortality (Fig. 4A). CC001 mice were fully resistant, with no or mild clinical signs (Fig. 4A, left and center). In contrast, all CC071 mice were moribund or dead by day 10 p.i., with early and quickly aggravating symptoms, almost like those in 129-*Ifnar1* mice. Only one of the five CC005 mice developed symptoms and died. The peak viral load (day 2 p.i.) varied over a  $2.4\text{-log}_{10}$  range, and the differences between strains were similar to those observed with the FG15 ZIKV strain (Fig. 3B). Here again, the plasma viral load at day 2 p.i. was



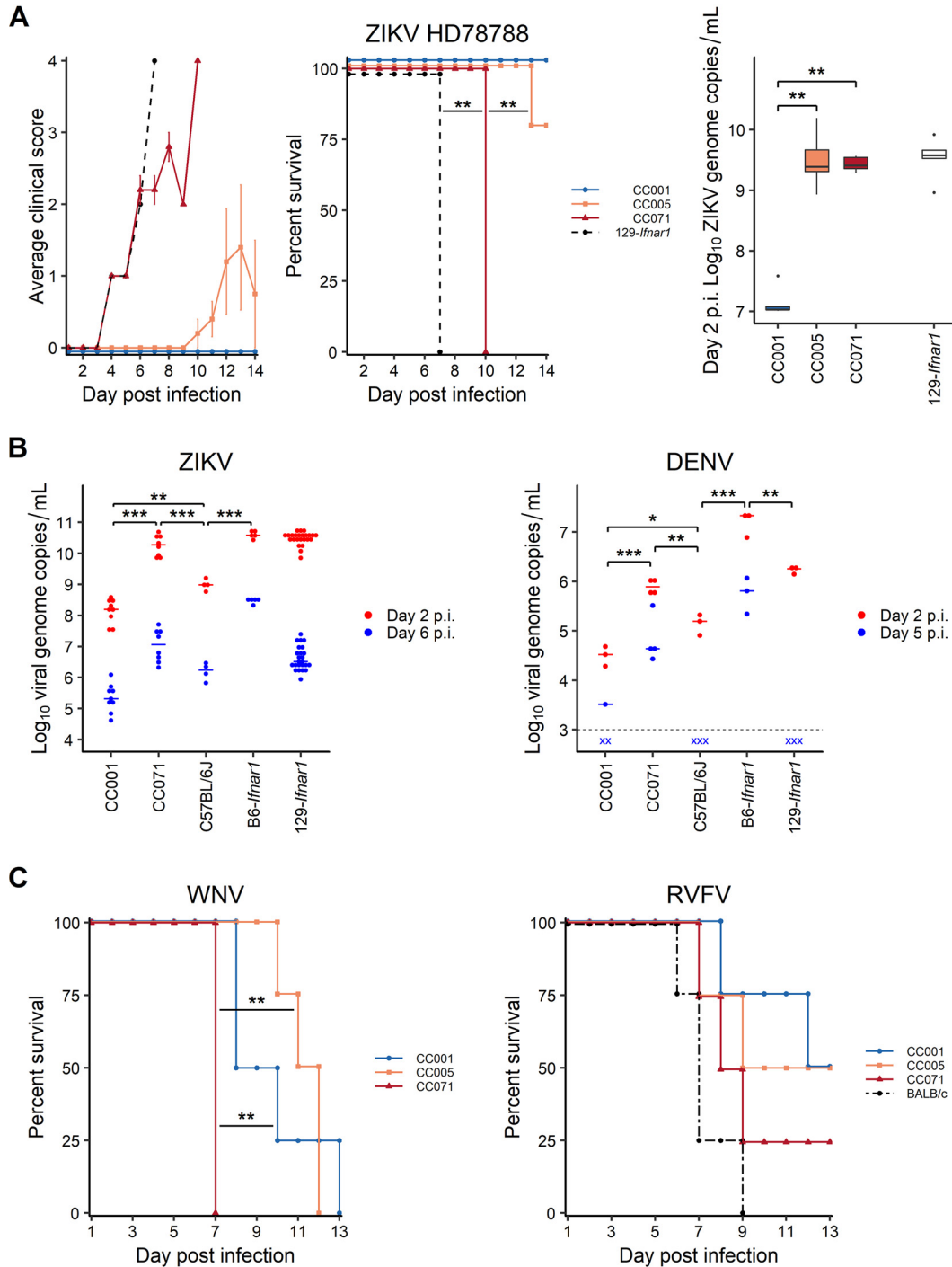


**FIG 4** The differences in susceptibility to ZIKV between CC strains correlate with the differences in susceptibility to other flaviviruses. (A) Six- to 8-week-old mice from three selected CC strains treated with the MAR1-5A3 MAb and 129-*Ilnar1* mice were infected intraperitoneally with  $10^3$  FFUs of ZIKV HD78788. (Left) Average clinical score, with numerical values given as described in the legend to Fig. 1; (center) Kaplan-Meier survival curves (log-rank test); (right) plasma viral load at day 2 p.i., measured by RT-qPCR (*P* values were determined by the Wilcoxon rank-sum test). (B) The viral loads after ZIKV infection (left; data extracted from Fig. 3) and DENV infection (right; data for i.v. infection with  $2 \times 10^6$  FFUs of DENV KDH0026A) in MAb-treated 6- to 8-week-old CC001, CC071, and B6 mice and in 129-*Ilnar1* and B6-*Ilnar1* were compared (*P* values were determined by the *t* test). (C) (Left) Kaplan-Meier survival curves for four 8- to 12-week-old male mice of each of the three selected CC strains infected i.p. with 1,000 FFUs of WNV strain IS-98-ST1 and monitored for 14 days (*P* values were determined by the log-rank test); (right) Kaplan-Meier survival curves for four to five 8- to 12-week-old male mice of the BALB/cByJ strain and each of the three selected CC strains infected i.p. with 100 PFUs of RVFV strain ZH548 and monitored for 14 days (log-rank test, *P* > 0.05). \*, *P* < 0.05; \*\*, *P* < 0.01; \*\*\*, *P* < 0.001.

the highest in the very susceptible CC071 and 129-*Ifnar1* strains and low in the resistant CC001 strain, but it was also very high in CC005 mice, which were moderately susceptible, confirming that clinical severity does not depend solely on the peak plasma viral load.

To evaluate whether these differences in susceptibility were specific to ZIKV or extended to other flaviviruses, we assessed the phenotypes of a few strains after infection with DENV and WNV, two other members of the *Flaviviridae* family.

We measured the plasma viral load after intravenous (i.v.) infection with  $2 \times 10^6$  FFUs of DENV DKH0026A (a DENV serotype 1 [DENV-1] strain) in MAb-treated CC001, CC071, and B6 mice and in 129-*Ifnar1* and B6-*Ifnar1* mice (Fig. 4B, right). Most interstrain differences observed with the ZIKV FG15 strain (Fig. 4B, left, with data from Fig. 3B) were also observed with DENV, with the CC071 mice displaying the highest plasma viral load after MAb treatment. DENV infection was, overall, much less clinically severe, since only B6-*Ifnar1* mice developed nonlethal symptoms, including ruffled fur, hunched back, and ataxia.

We also investigated the susceptibility of the selected CC strains to WNV. *Oas1b* was previously shown to be a major host genetic determinant of susceptibility to WNV in mice (62). Of note, the three selected CC strains carry the same truncated, nonfunctional allele of *Oas1b* inherited from the laboratory strain founders (Table 1), conferring to them susceptibility to WNV infection. CC mice were infected i.p. with  $10^4$  FFUs of WNV IS-98-ST1 and monitored for 14 days p.i. (efficient WNV infection does not require anti-IFNAR MAb treatment in mice carrying the truncated *Oas1b* allele). All CC071 mice died by 7 days p.i., which was significantly faster than the time to death for the CC001 and CC005 mice (log-rank test,  $P < 0.01$ ) (Fig. 4C, left), indicating that the genetic diversity between CC strains also influences their susceptibility to WNV even in the context of *Oas1b* deficiency.

To assess whether the differences in susceptibility between these CC strains also applied to other viruses, we infected them with  $10^2$  PFU of Rift Valley fever virus (RVFV) ZH548 i.p. No significant difference was found between the three CC strains (log-rank test,  $P > 0.3$  for all pairwise comparisons) (Fig. 4C, right), which succumbed late in the infection, like the commonly used BALB/cByJ mice. Only CC001 mice died significantly later than BALB/cByJ mice (log-rank test,  $P = 0.04$ ).

**Genetic analysis suggests polygenic control of susceptibility to ZIKV in CC mice.** To identify host genetic factors controlling the susceptibility to ZIKV in the CC strains, we performed a genome-wide association study between the plasma viral loads at days 2 and 6 p.i. or the rate of decrease in the plasma viral load and the genotypes of the 35 CC strains. Genetic associations were plotted as logarithm of the odds (LOD) scores. We did not find any genome locations at which the LOD scores reached the minimum 0.1 significance threshold for any of the three traits (Fig. 5), which would be expected if phenotypic variations were controlled by one or two loci with strong effects. Therefore, these results suggest that the plasma viral load is controlled by multiple small-effect genetic variants.

**The genetic diversity of CC strains controls brain viral load and pathology.** To assess the influence of host genetics on the brain pathology caused by ZIKV infection, we further characterized the three previously selected CC strains. We measured the viral load in the brain 6 days after i.p. infection with ZIKV FG15 in MAb-treated CC mice and 129-*Ifnar1* mice (Fig. 6A). CC005 and CC071 mice, which had higher peak plasma viral loads than CC001 mice, also had higher brain viral loads (mean =  $6.5 \log_{10}$  copies/ $\mu$ g RNA for CC005 and CC071 mice, compared with  $5 \log_{10}$  copies/ $\mu$ g RNA for CC001 mice). As expected, 129-*Ifnar1* mice showed the highest viral load in the brain. These results indicate an overall correlation between plasma and brain viral loads.

Histopathological analysis, carried out with brain tissue from the same mice (Fig. 6B to N), revealed different lesion profiles between the four mouse strains (Fig. 6B, F, I, and L for low-magnification images). 129-*Ifnar1* mice clearly displayed the most severe inflammatory lesions with subacute leptomeningoencephalitis (i.e., infiltration of

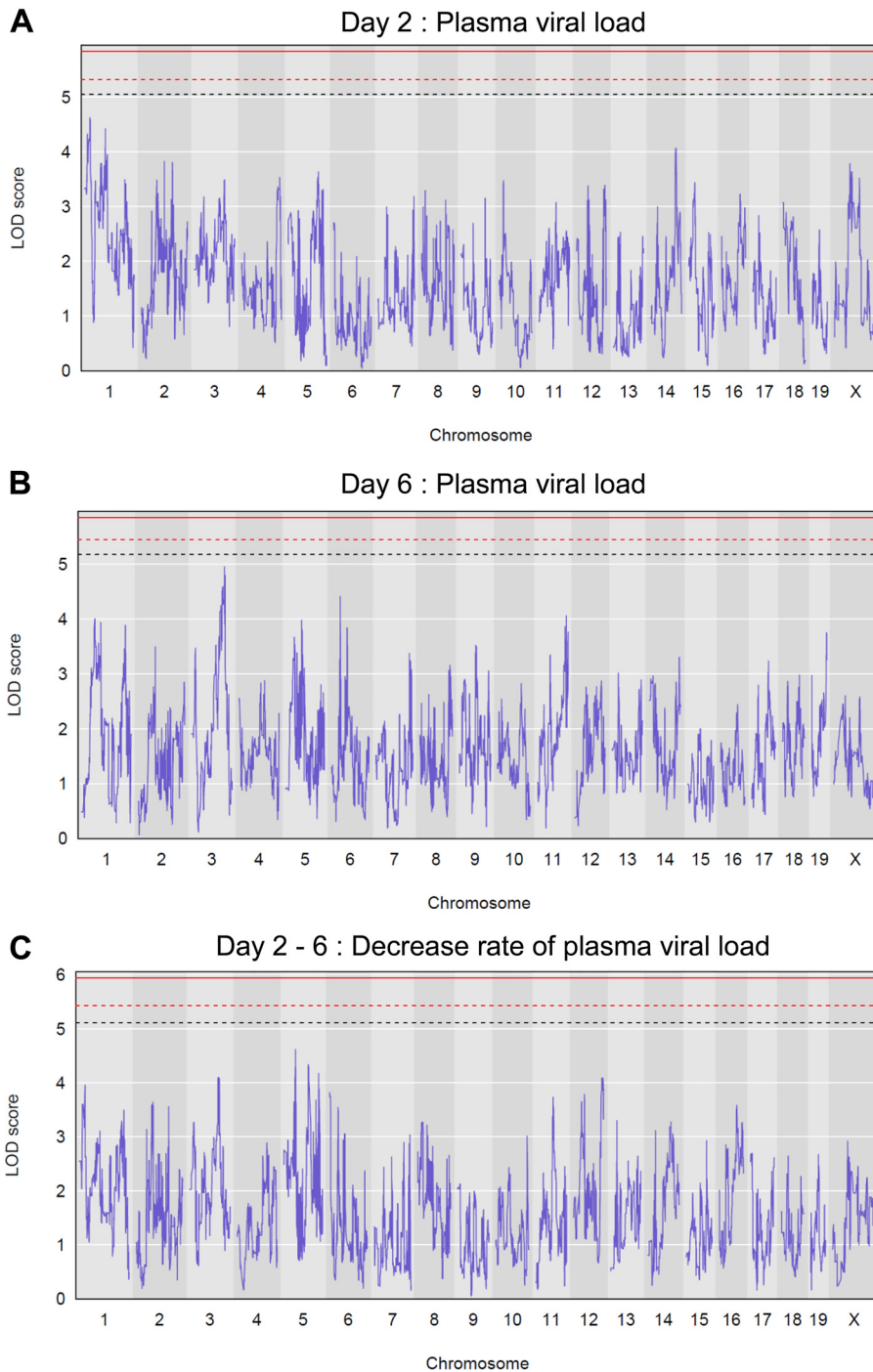


**FIG 5** Genetic analysis of susceptibility to ZIKV fails to identify simple genetic control. Genome-wide linkage analysis for the plasma viral load at day 2 p.i. (A), the plasma viral load at day 6 p.i. (B), and the rate of decrease in the plasma viral load (C) for the 35 CC strains for which the results are shown in Fig. 3. The x axis represents the genomic location; the y axis is the LOD score, representing the statistical association between the phenotype and the genomic location. Genome-wide thresholds of  $P$  equal to 0.1, 0.05, and 0.01, computed from 1,000 permutations, are represented by dashed black, dashed red, and plain red lines, respectively. No genome location reached the threshold of  $P$  equal to 0.05.

perivascular spaces and leptomeninges by lymphocytes, plasma cells, and macrophages; Fig. 6B to E) and activation of microglial cells with microglial nodules (Fig. 7B to D). In contrast, almost no histological lesions were detected in the brains of CC001 mice (Fig. 6F to H), which showed normal, nonactivated, microglial cells (Fig. 7E to G).

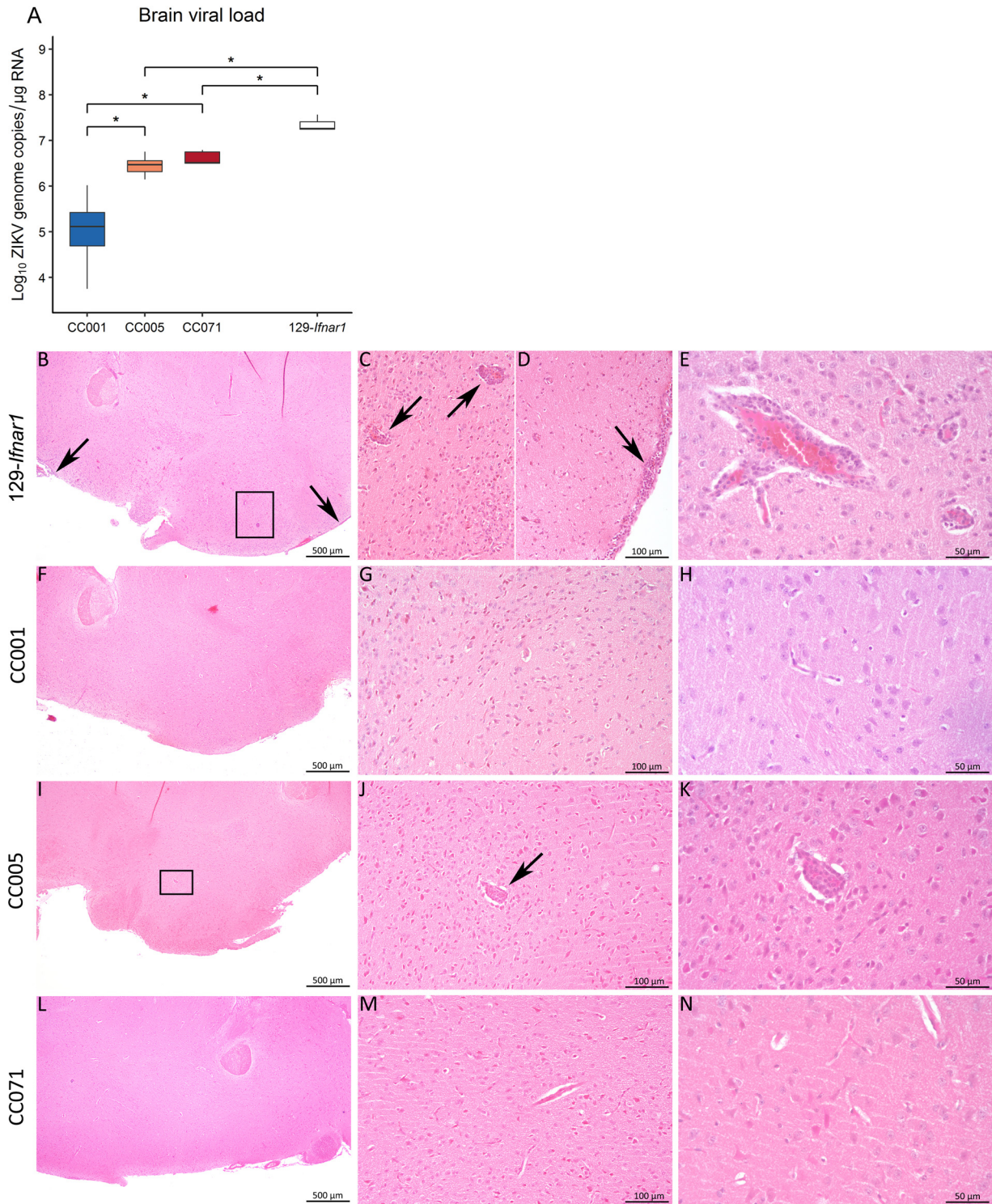


**FIG 6** Genetic variations between CC strains control the brain viral load and histological profile in infected mice. Four to five 6- to 8-week-old mice of the 129-*Irfnar1* strain and three selected CC strains were infected i.p. with  $10^7$  FFUs of ZIKV FG15 24 h after i.p. injection of 2 mg of the MAR1-5A3 MAb. (A) Brain viral load measured by RT-qPCR at day 6 p.i. \*,  $P < 0.05$ , Wilcoxon rank-sum test. (B to N) Representative HE-stained brain sections at three different magnifications. (B to E) 129-*Irfnar1* mice ( $n = 3$ ). Black rectangle, encephalitis with perivascular lymphocyte cuffs. (B and D) Arrows, lesions of subacute leptomeningoencephalitis. (C) Arrows, perivascular lymphocyte cuffs. (F to H) CC001 mice ( $n = 5$ ). (I to K) CC005 mice ( $n = 5$ ). Black rectangle, encephalitis with perivascular lymphocyte cuffs; arrow, perivascular cuffing. (L to N) CC071 mice ( $n = 4$ ).

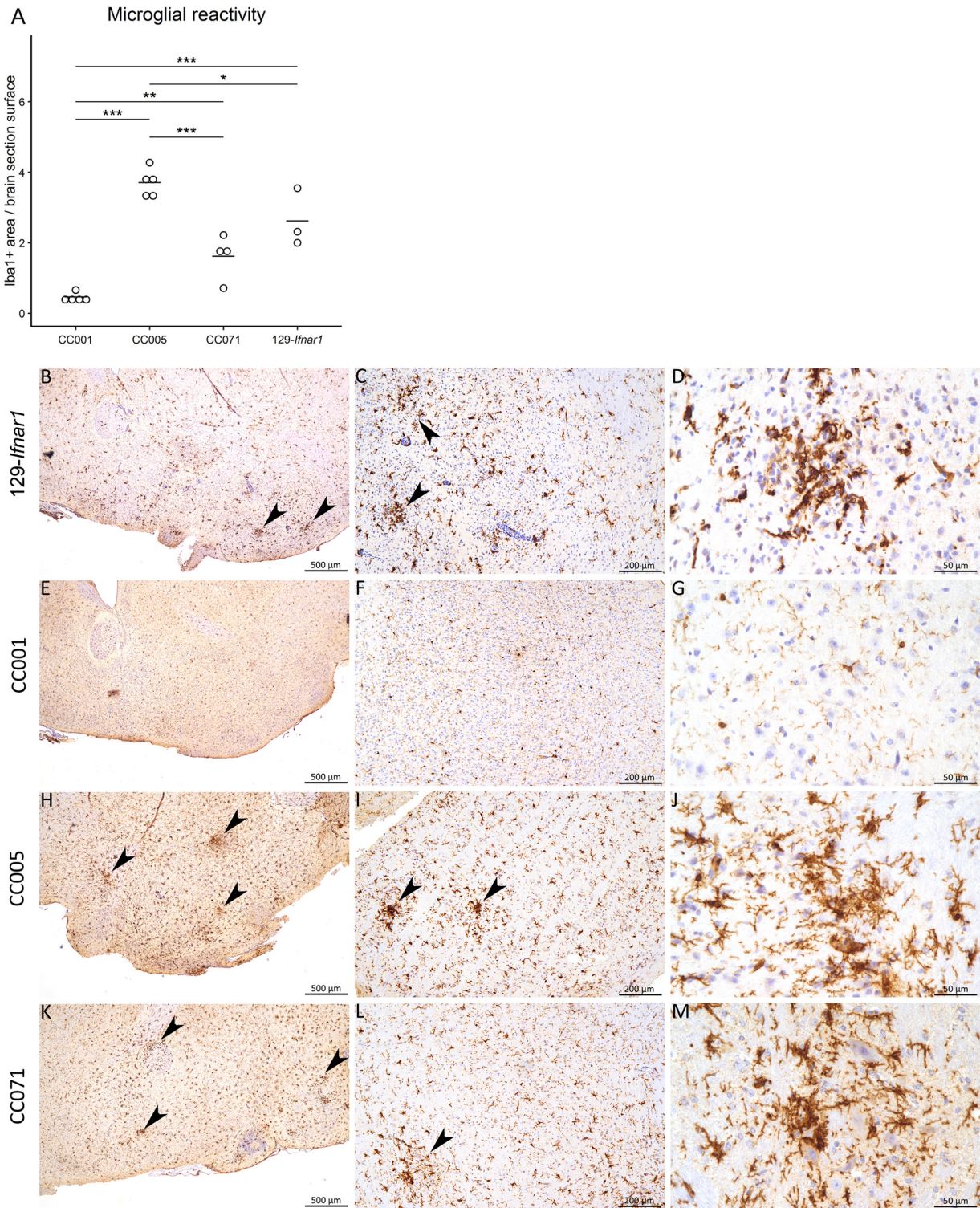


**FIG 7** Genetic variations between CC strains control brain neuroinflammation in infected mice. Microglial reactivity was assessed on brain sections from the same mice described in the legend to Fig. 6 by anti-Iba1 immunohistochemistry. (A) Quantification of the Iba1 labeling signal on the brain sections. *P* values were determined by *t* tests. \*, *P* < 0.05; \*\*, *P* < 0.01; \*\*\*, *P* < 0.001. (B to M) Representative anti-Iba1 immunohistochemistry of brain sections at three different magnifications. (B to D) 129-Ilfnar1 mice (*n* = 3); (E to G) CC001 mice (*n* = 5); (H to J) CC005 mice (*n* = 5); (K to M) CC071 mice (*n* = 4). Arrowheads, nodules of activated microglial cells.

Only very rare small clusters of activated microglial cells were detected. CC005 mice displayed moderate inflammatory lesions characterized by perivascular cuffing (Fig. 6I to K) and activation of microglial cells (hyperplasia and thickening of cell processes) and microglial nodules (Fig. 7H to J). CC071 mice displayed almost no lesions upon hematoxylin-eosin (HE) staining (Fig. 6L to N) but inflammatory lesions of intermediate severity with activation of microglial cells and microglial nodules (Fig. 7K to M) similar to those in 129-*Irfnar1* mice (Fig. 7A), as revealed by Iba1 immunolabeling.

The nature and intensity of brain histological lesions may depend on the circulating viral load, on the capacity of the virus and of the MAb to cross the blood-brain barrier, and on the permissiveness of brain cells (in particular, neurons and microglia). To assess the differences in the susceptibility of brain cells between CC strains, we performed intracerebral (i.c.) infections to deliver the virus directly into the brain tissue. 129-*Irfnar1* and MAb-untreated CC mice received  $10^5$  FFUs of ZIKV FG15 in the left ventricular region of the brain and were followed for 3 weeks. Mild and transient symptoms (ruffled fur, hunched back) were observed in a few mice of the three strains, and one CC005 mouse died on day 19 p.i. A second group of CC mice was infected similarly and euthanized at day 6 p.i. for histological analysis. The differences in the brain viral loads between CC strains were similar to those observed after i.p. infection, with CC005 and CC071 mice showing significantly higher brain viral loads than CC001 mice (Fig. 8A). The lesions seen in 129-*Irfnar1* mice after infection by the i.c. route were mostly similar to the lesions seen after infection by the i.p. route, with marked subacute leptomeningoencephalitis (Fig. 8B to E) and activation of microglial cells (Fig. 9B to D). In contrast, the lesion profiles were clearly different in the three CC strains. Two of the five CC001 mice displayed no significant histological lesions, with normal resting microglial cells, while the other three displayed minimal lesions, with gliosis (Fig. 8F to H) and rare small clusters of activated microglial cells (Fig. 9E to G). By the i.c. route of infection, CC005 mice displayed heterogeneous lesion profiles, with either suspected meningitis and gliosis (Fig. 8I to K; 4/5 mice) or moderate leptomeningoencephalitis (1/5 mice). Activation of microglial cells with variable severity was detected in all animals (Fig. 9H to J). Strikingly, all CC071 mice displayed marked leptomeningoencephalitis (Fig. 8L to O), with the strongest activation being of microglial cells (Fig. 9A and K to M).

These results indicate that CC strains differ in their permissiveness to viral replication in the brain and in their susceptibility to ZIKV-induced histological brain damage. The comparison between the i.p. and i.c. infection routes shows that these variations cannot be explained only by the possibility of the differential dissemination of ZIKV from the circulation to the brain between CC strains.

**Viral replication in CC071 mouse cells is increased *in vitro*.** The differences in the peak plasma viral loads and the results from i.c. infections suggested that different efficiencies of viral replication could contribute to the variations in susceptibility between CC strains. To address this point, we measured the production of infectious viral particles in MEFs derived from the CC001 and CC071 strains. Cells were infected with ZIKV FG15 at a multiplicity of infection (MOI) of 5. While the viral titers remained stable in CC001 mice between 24 and 72 h, the production of viral infectious particles by CC071 MEFs increased very significantly over the same period (Fig. 10). These results suggest that the increased replication efficiency in CC071 mice could contribute to their susceptible phenotype.

## DISCUSSION

ZIKV is a serious public health concern, considering the occurrence of severe neurological complications in adults and the congenital malformations that can result from the infection of pregnant women. The variable outcomes of ZIKV infection in humans have led investigators to hypothesize a role for host genetic factors (9, 13), although this has never been demonstrated thus far. Like for other infectious diseases, human genetic studies on susceptibility to ZIKV would require large cohorts of patients and would be confounded by pathogen genetics, pathogen dose, mosquito-dependent

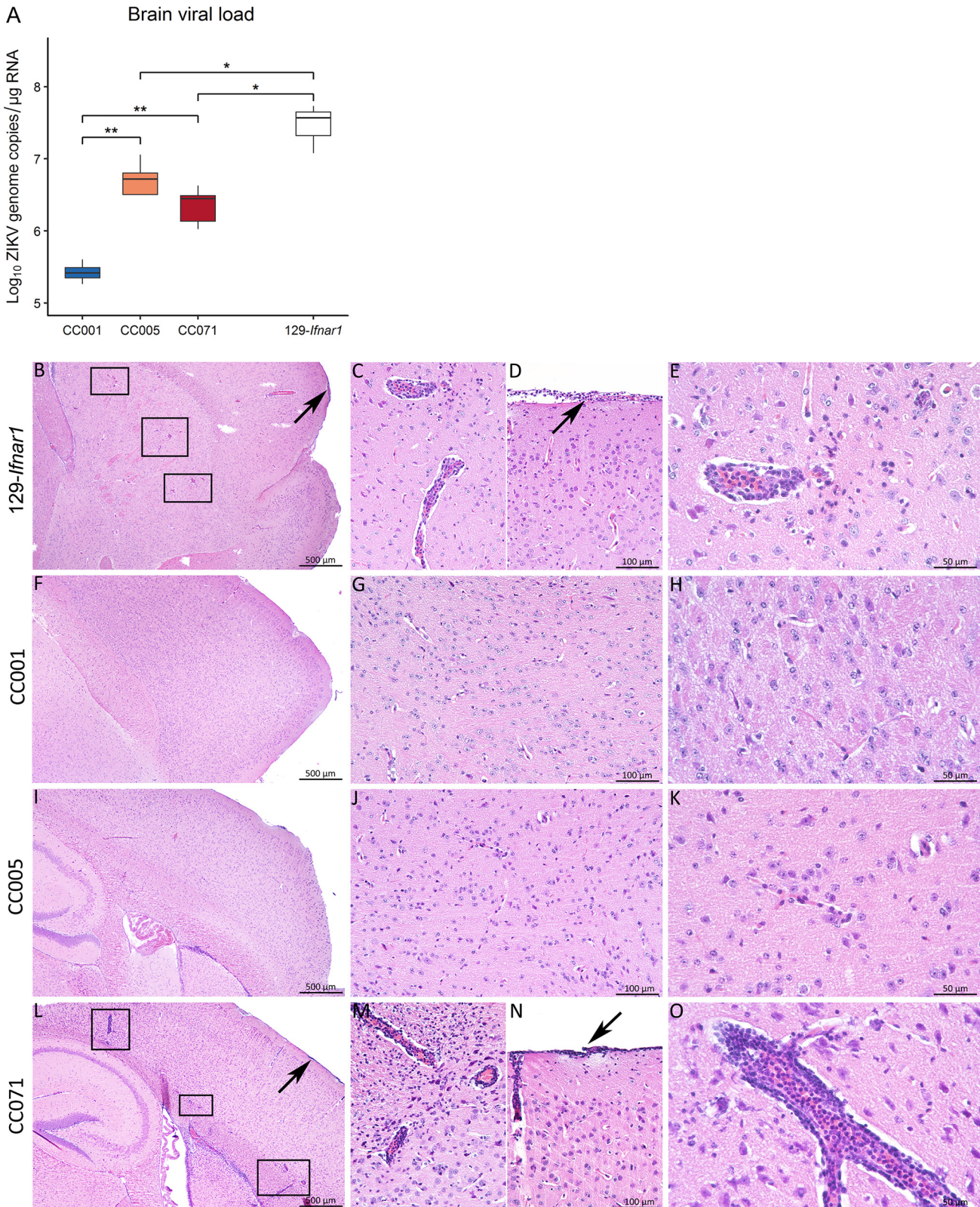


**FIG 8** Intracranial ZIKV FG15 infection results in a strain-dependent viral load and brain histological lesions. Groups of 5- to 6-week-old mice of the 129-*Irfar1* strain and three selected CC strains (3 to 5 mice per strain) were infected i.c. with  $10^5$  FFUs of ZIKV FG15 in the absence of prior anti-IFNAR treatment. (A) Brain viral load measured by RT-qPCR at day 6 p.i. *P* values were determined by the Wilcoxon rank-sum test. \*, *P* < 0.05; \*\*, *P* < 0.01. (B to O) Representative HE-stained brain sections at three different magnifications. (B to E) 129-*Irfar1* mice (*n* = 4). Black rectangles, encephalitis with perivascular lymphocyte cuffs; arrows, leptomeningitis. (F to H) CC001 mice (*n* = 5). (I to K) CC005 mice (*n* = 4). (L to O) CC071 mice (*n* = 5). Black rectangles, encephalitis with perivascular lymphocyte cuffs; arrows, leptomeningitis.

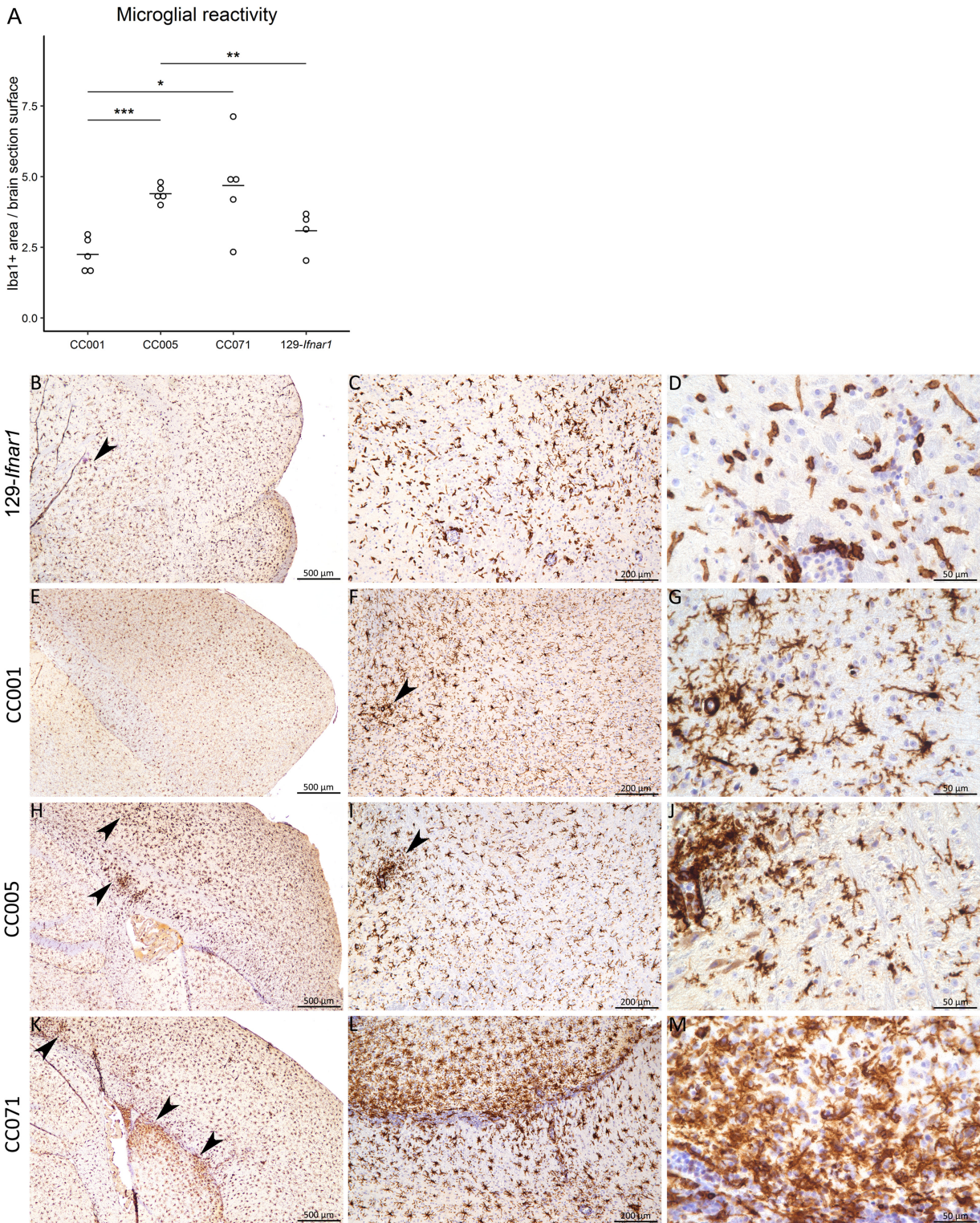


**FIG 9** Intracranial ZIKV FG15 infection results in strain-dependent neuroinflammation of the brain. Microglial reactivity was assessed on brain sections from the same mice described in the legend to Fig. 8 by anti-Iba1 immunohistochemistry. (A) Quantification of the Iba1 labeling signal on the brain sections. *P* values were determined by *t* tests. \*, *P* < 0.05; \*\*, *P* < 0.01; \*\*\*, *P* < 0.001. (B to M) Representative anti-Iba1 immunohistochemistry of brain sections at three different magnifications. (B to D) 129-Ilfar1 mice (*n* = 4); (E to G) CC001 mice (*n* = 5); (H to J) CC005 mice (*n* = 4); (K to M) CC071 mice (*n* = 5). Arrowheads, nodules of activated microglial cells.



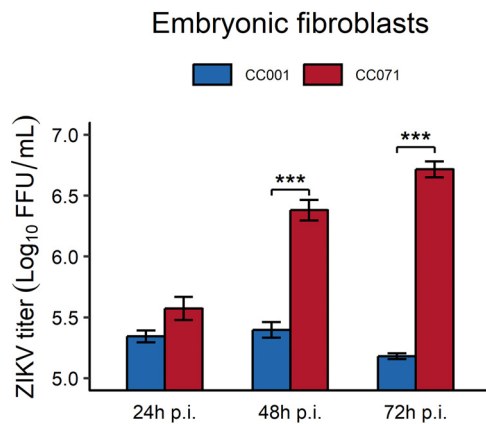


**FIG 10** Enhanced ZIKV replication in CC071 MEFs compared with CC001 MEFs. MEFs derived from CC001 and CC071 mouse embryos were infected with ZIKV FG15 at an MOI of 5. The ZIKV titer in the supernatant was quantified by a focus-forming assay at 24, 48, and 72 h p.i. The data represent the mean  $\pm$  SEM from 3 biological replicates. The results were replicated in 3 independent experiments (*t* tests, \*\*\*,  $P < 0.001$ ).

factors, and multiple environmental parameters. Also, genetic analyses are complicated by the randomness of virus infections and heterogeneity in clinical assessment.

Several mouse models of human ZIKV infection have already been described and have substantially improved our understanding of viral tropism, dissemination, pathogenesis, persistence, transmission, and vaccine protection. To overcome the inability of ZIKV to inhibit IFN induction and signaling pathways in mice, as was observed in humans (27), most studies have been performed using *Ifnar1*-deficient mice, which have become a reference model. However, high levels of viral replication can also be achieved by temporary inhibition of IFN signaling by anti-IFNAR MAb treatment (30, 31, 63) or even in immunocompetent mice by infecting neonates (36, 64–66) or using a combination of mouse-adapted ZIKV strains and human STAT2-knock-in mice (67).

The choice of ZIKV strain used in an animal model is important to maximize the relevance of mouse studies to human infection. Previous mouse studies have used different ZIKV strains from the African or Asian lineage. Mouse-adapted strains of the African lineage derived from a large number of serial passages are more pathogenic in mice at lower doses than strains of the Asian lineage (34) but carry mutations that may bias the translatability of the results to humans. To avoid this limitation, mouse studies have often used different ZIKV strains derived from clinical isolates of the Asian lineage. Genetic differences between these two lineages are suspected to be responsible for the emergence of symptomatic cases in humans starting with the Yap Island epidemics in 2007 (7, 8). Therefore, while the ZIKV strain needs to be standardized in experimental studies, for generalization of the results obtained with one viral strain, those results must be confirmed using another viral strain. Because of the incidence of neurological complications associated with infections caused by strains of the Asian lineage of ZIKV, we used for our genetic screening a low-passage strain derived from a 2015 case in French Guiana, at an early stage of the South American epidemics. Since this strain had not been adapted to the mouse, high doses were required to achieve high circulating viral loads.

Most mouse studies have used either B6-*Ifnar1* or 129-*Ifnar1* strains without a specific rationale, and their results cannot be directly compared due to many experimental differences, such as the ZIKV strain, dose, and route of inoculation (35). Under strictly identical conditions, we found that B6-*Ifnar1* mice developed more rapid and severe clinical symptoms and higher mortality than 129-*Ifnar1* mice, despite similar levels of plasma viral RNA at day 2 p.i. We also found that the viral load persisted longer in B6-*Ifnar1* mice. These results show that, under our experimental conditions, these two *Ifnar1*-deficient strains have clearly distinct susceptibilities to ZIKV. To our knowledge,

these two strains have been compared in only one study, which found no difference in survival after WNV infection (68). However, their extreme susceptibility might have prevented the identification of any difference. Our results have practical implications for many studies based on *Ifnar1*-deficient mice and motivate further genetic studies to identify the determinants and mechanisms controlling differences in susceptibility between B6 and 129 mouse inbred backgrounds.

To further investigate the role of host natural genetic variants on ZIKV susceptibility, we leveraged the genetic diversity across CC strains. The CC has been developed as a collection of inbred strains that more accurately reproduce the genetic diversity and phenotypic range seen in the human population (69). To enable systemic ZIKV replication after parenteral inoculation in mice with diverse genetic backgrounds, we blocked the type I IFN response using the MAR1-5A3 MAb (23, 31).

Several lines of evidence demonstrate that the MAb treatment was effective in all CC strains. First, we showed a similar abrogation of IFN- $\alpha$ -induced STAT1 phosphorylation in MEFs from B6 mice and two CC strains carrying the most divergent *Ifnar1* haplotypes (Fig. 2A). Moreover, the differences in the peak plasma viral load across 35 CC strains were not associated with the *Ifnar1* allele that each CC mouse strain received from the founder strains. Second, the peak viral load in all MAb-treated CC mice was at least 2.5 logs higher than that in untreated CC071 mice (Fig. 2B and 3B). Finally, we showed, in two CC strains, that increasing the dose of MAb to 4 mg did not modify the plasma viral loads at days 2 and 6 p.i. (Fig. 2F), indicating that the 2-mg dose was not limiting. This is consistent with the 5.2-day half-life of the MAR1-5A3 antibody previously reported (30). These results validate that the MAR1-5A3 MAb is effective across a broad range of mouse genetic backgrounds, which will be useful for the development of new models of viral infections.

A single injection of the MAR1-5A3 MAb at 24 h before ZIKV infection resulted in moderate to very high levels of viral RNA in the blood and brain. ZIKV infection was symptomatic in a minority of CC strains (3/35), as has been observed in infected humans (9, 70), and mortality was observed only in CC071 mice. These results confirm that ZIKV can replicate and establish viremia without inducing symptoms (29). Moreover, while all symptomatic strains had high peak viral loads, other strains with similarly high viral loads (like the CC005 or CC061 strains) never developed any signs of acute illness, indicating that other pathogenic mechanisms are required to result in symptomatic infection and that the viral load alone does not reliably predict the clinical outcome of ZIKV infection in a genetically diverse mouse population.

Since all experimental parameters were carefully standardized between strains (in particular, the microbiological environment in which they were bred), which resulted in small intrastrain variations, and since the MAR1-5A3 MAb treatment was effective across all CC strains, differences in peak viral loads between strains can be confidently attributed to host genetic variants. The 86% broad-sense heritability further indicates that the genetic background is the principal factor driving the peak viral load across CC strains.

Viremia decreased between days 2 and 6 p.i., as previously reported in several studies (56, 71, 72) but not in others (29, 57), for reasons that have not been discussed and that remain unclear. In our study, the rate of decrease, which was estimated as the difference of the  $\log_{10}$  plasma viral load between day 2 and day 6 p.i., showed remarkable homogeneity between individuals of the same CC strain and very large variations across CC strains. Injecting additional doses of MAb during the course of infection did not modify the kinetics of the viral load (Fig. 2F), ruling out the potential role of differential rates of antibody turnover. These results demonstrate a strong influence of host genes on the rate of ZIKV clearance from the bloodstream. The decrease in the circulating viral load is the net result of ZIKV production in infected tissues, dissemination to the bloodstream, and elimination from the circulation. Therefore, host genes could control the kinetics of the viral load through multiple mechanisms.

After exploring the range of susceptibility to ZIKV across a broad range of genetic

diversity, we focused our study on a few CC strains exhibiting contrasting phenotypes with the aim of characterizing new models (54). The CC001 strain was one of the strains least permissive to ZIKV, with a low peak viral load. At the other extreme of the distribution, the CC005 and CC071 strains had similarly high plasma viral loads, while only the CC071 strain showed symptoms and high mortality. These differences between CC strains were strikingly conserved with the African, mouse-adapted, HD78788 strain (Fig. 4A). The use of lower infectious doses with the HD78788 virus was supported by its higher pathogenicity resulting from mouse adaptation. The consistency between these two experiments suggests that the large phenotypic diversity that we have reported should apply to most ZIKV strains.

Overall, the brain viral load and brain pathology after i.p. infection were consistent with the peak plasma viral load. In CC mice, the most notable microscopic lesions included signs of neuroinflammation, evidenced by Iba1 immunohistochemistry. Neuroinflammation was similar in 129-*Irfnar1*, CC005, and CC071 mice. These changes were less pronounced than those in a previous study, which reported more severe central nervous system lesions in MAR1-5A3-treated B6 mice (31) infected with a more virulent African lineage ZIKV strain. The variable severity of the lesions observed in CC mice, ranging from very mild abnormalities in CC001 mice to inflammatory lesions with perivascular cuffing, activation of microglial cells, and microglial nodules in CC005 mice, indicates that the genetic background also controls ZIKV neuropathogenesis.

The less severe histological lesions observed in CC mice than in 129-*Irfnar1* mice could be due to the limited access to the brain of the virus or of the MAb, which does not appreciably cross the blood-brain barrier (29). Therefore, intracerebral infection aimed at comparing brain lesions between strains while controlling for the amount of virus effectively delivered. Surprisingly, CC001 and CC005 mice showed similar types and severities of lesions (although not all CC001 mice showed lesions), while CC071 mice developed much more severe signs of leptomeningoencephalitis with massive neuroinflammation, similar to those seen in 129-*Irfnar1* mice. This last result suggests that the milder lesions observed in CC071 mice than in 129-*Irfnar1* mice after i.p. infection were likely due to reduced viral dissemination to the brain. Importantly, mice did not receive prior MAb treatment, allowing for the development of local and systemic antiviral responses. These results emphasize the complex interplay between infected cells and effectors of the immune response, which likely differs between CC strains under the control of host genes.

The viral replication rate was investigated in resistant CC001 mice and highly susceptible CC071 mice, as it is a plausible mechanism for the differences in susceptibility between these two strains. MEFs are a semipermanent source of cells which have been extensively used to assess viral replication (73, 74), including with ZIKV (75, 76). In CC001 MEFs, the production of infectious viral particles was stable between 24 and 48 h and decreased between 48 and 72 h, while it steadily increased over time in CC071 MEFs, leading to significantly higher viral titers starting at 48 h. Our data are consistent with the observation by Caires-Junior et al., who reported an increased ZIKV replication rate in induced pluripotent stem cell-derived neuroprogenitor cells from CZS-affected babies compared with their unaffected dizygotic twins (13). Therefore, our results strongly suggest that the increased replication rate in CC071 mice compared with CC001 mice likely contributes to their higher plasma and brain viral loads and to their higher overall susceptibility to ZIKV.

Investigating the genetic diversity of a large number of CC strains has significantly extended the range of phenotypes induced by ZIKV infection in mice, and these mice better model the heterogeneity of the human population. It has allowed the testing of important factors, such as mouse gender and the method of viral load measurement across multiple host genetic backgrounds, providing robust conclusions (37). Importantly, we found no differences between male and female mice in susceptibility to ZIKV disease or in the peak viral load (Fig. 2E). We also found a high correlation between the viral loads measured by titration and by qRT-PCR over a 2- $\log_{10}$  range (Fig. 2D). This is in contrast to the findings of a study of Ebola virus, which showed that, in spleen and

**TABLE 3** Summary of main features of ZIKV infection in MAb-treated CC strains and 129-*Irfar1* mice<sup>a</sup>

Mouse strain	Symptoms	Mortality (%)	Peak plasma viral load	Rate of decrease of plasma viral load	Systemic infection		Intracerebral infection		Viral replication <i>in vitro</i> (24–72 h)
					Brain viral load	Brain pathology	Brain viral load	Brain pathology	
CC001	–	0	+	Moderate	+	–	+	++	Decreasing
CC005	–	0	+++	Fast	+++	+++	+++	+++	ND
CC071	+++	78	+++	Moderate	+++	++	+++	++++	Increasing
129- <i>Irfar1</i>	++	12.50	+++	Fast	+++	+++	+++	++++	ND

<sup>a</sup>–, absent; +, ++, +++, and +++++, present at increasing levels; ND, not done.

liver, the susceptible mice produced similar amounts of viral genomes but 1 to 2 log<sub>10</sub> more infectious virions than the resistant mice (43).

Genetic diversity also allowed us to assess the correlations between traits, which cannot be achieved with a single strain. We showed that the brain viral load at day 6 after i.p. infection was consistent with the plasma viral load at day 2 p.i. but that the plasma viral loads at days 2 and 6 p.i. were only moderately correlated. Likewise, we found that clinical severity did not correlate with the intensity of brain histological lesions and neuroinflammation, as summarized in Table 3. These dissociations between phenotypes provide evidence for partly distinct mechanisms and genetic control (37) and lead to distinct mouse models.

A recent study has reported strain-dependent variations in the long-term neuropathological and behavioral consequences of ZIKV infection after neonatal infection between four mouse inbred strains known to differ in their susceptibility to pathogens (36). Since they are all laboratory strains, they do not cover the same genetic variation used in our study, and it is likely that even more diverse phenotypes would be observed in this model with the CC panel.

Genetic analysis of our results strongly suggests that, in contrast to other viruses for which major host genetic determinants have been identified (e.g., *Oas1b* for WNV [62] or *Mx1* for influenza virus [77]), susceptibility to ZIKV in CC strains is under polygenic control. This is supported by the continuous distributions, across the CC strains, of the values of the peak plasma viral load (Fig. 3B) and of the rate of viral decrease (Fig. 3C) and by the absence of any regions of the genome significantly associated with variations in viral loads (Fig. 5). Calculations based on the CC genotypes show that, with 35 strains and an average of 5 mice per strain, we had an 80% power to detect a biallelic quantitative trait locus (QTL) explaining 30% or more of the phenotypic variance (78). This clearly rules out the possibility that the phenotypic variations measured across CC strains were controlled by one or a few genes with major effects, as observed with *Oas1b* for WNV (47). Dissecting the genetic architecture of resistance and susceptibility to ZIKV in these strains will require combining complementary strategies. Intercrosses between contrasted strains, such as strains CC001 and CC071, will reduce the genetic complexity and may result in an increased power for QTL mapping due to the larger sample size (54). However, the mapping resolution achieved in an F2 hybrid or a backcross leads to large genetic intervals. Other approaches, such as gene expression studies on various cell types (such as immune cells, neurons, or glial cells) will be used to identify differentially activated host response pathways and reduce the number of candidate genes in these intervals.

*Oas1b* is an interferon-stimulated gene and a major determinant of mouse susceptibility to WNV (45). A variant in *OAS3*, a member of the gene family in humans homologous to *Oas1b*, has been associated with an increased severity of dengue (79). Most laboratory strains, including five of the eight CC founders, carry the same nonfunctional allele of *Oas1b*, which renders them susceptible to WNV infection (62), while the three wild-derived CC founders carry polymorphic but functional alleles and are resistant (45). CC strains therefore carry either functional or nonfunctional *Oas1b* alleles. Our results provide multiple lines of evidence to rule out the possibility of a significant role of *Oas1b* in the variations in susceptibility to ZIKV across CC strains. First,

since MAb-mediated blockade of the type I IFN response likely temporarily inhibits *Oas1b* induction, the *Oas1b* allele is unlikely to explain the differences in the peak viral load at day 2 p.i. Moreover, our QTL mapping analysis showed that the mouse genotype at *Oas1b* (located on distal chromosome 5) did not significantly contribute to variations in the viral load at day 2 or day 6 p.i. or in the rate of viral load decrease (Fig. 5). Finally, since the CC001, CC005, and CC071 strains carry the *Oas1b* truncated allele (Table 1), the differences in clinical severity, brain pathology, and replication rate in infected cells among these strains must be controlled by other genetic variants. Interestingly, because of the large difference in the survival times after WNV infection between CC071 mice and CC001 or CC005 mice, these strains provide ideal strain combinations to identify novel genes controlling susceptibility to this virus.

Out of this large series of CC strains, we identified several new mouse models of ZIKV disease. CC071 mice were the most susceptible to ZIKV infection and were more susceptible than MAb-treated B6 mice (Fig. 3A and B). MAb treatment was required to achieve a high circulating viral load (Fig. 2B), showing that CC071 mice have a functional type I IFN response. CC071 mice were also very susceptible to DENV and WNV, two flaviviruses related to ZIKV. However, they are not uniformly susceptible to infectious agents, since they showed susceptibility to RVFV similar to that of BALB/c, CC001, and CC005 mice and intermediate susceptibility to *Salmonella enterica* serovar Typhimurium (52). Together with other susceptible strains, like CC021 and CC026, which developed symptoms, or CC005, which developed severe brain lesions, CC071 mice will help identify the mechanisms of severe ZIKV infection and their genetic control. In contrast, CC001 mice were highly resistant, even to a strongly pathogenic African ZIKV strain, despite a blockade of type I IFN signaling. Extensive analysis of these CC strains with extreme phenotypes may elucidate how genetic variants affect susceptibility as well as innate and adaptive immune responses to flaviviral infection (54) and provide a deeper understanding of the pathophysiology of severe complications of human ZIKV disease.

## MATERIALS AND METHODS

**Mice.** All Collaborative Cross (CC) mice (purchased from the Systems Genetics Core Facility, University of North Carolina, and bred at the Institut Pasteur) (80), C57BL/6J mice (purchased from Charles River Laboratories France), and BALB/cByJ and *Irfar1*-knockout mice (mice with the *Irfar1*<sup>tm1Agt</sup> allele on the 129S2/SvPas or C57BL/6J background, designated 129-*Irfar1* and B6-*Irfar1*, respectively, and bred at the Institut Pasteur) were maintained under specific-pathogen-free conditions with a 14-h light and 10-h dark cycle and *ad libitum* food and water in the Institut Pasteur animal facility. All CC strains bred at the Institut Pasteur were included in this study. In all experiments, mice were killed by cervical dislocation. All experimental protocols were approved by the Institut Pasteur Ethics Committee (projects 2013-0071, 2014-0070, 2016-0013, 2016-0018, and dap190107) and authorized by the French Ministry of Research (decisions 00762.02, 7822, 6463, 6466, and 19469, respectively), in compliance with French and European regulations.

**Cell lines.** Vero cells (ATCC CRL-1586) were cultured at 37°C in Dulbecco's modified Eagle medium (DMEM; Gibco) supplemented with 10% fetal bovine serum (FBS; Eurobio). C6/36 cells (ATCC CRL-1660) were cultured at 28°C in Leibovitz medium (L-15 medium; Gibco) supplemented with 10% FBS, 1% nonessential amino acids (Life Technologies), and 1% tryptose phosphate broth (Life Technologies).

**Viruses.** The FG15 Asian Zika virus (ZIKV) strain, isolated from a patient during a ZIKV outbreak in French Guiana in December 2015, was obtained from the Virology Laboratory of the Institut Pasteur of French Guiana. The HD78788 African ZIKV strain, isolated from a human case in Senegal in 1991, was obtained from the Institut Pasteur collection. The KDH0026A DENV serotype 1 (DENV-1) strain, isolated from a patient in Thailand in 2010, was previously described (81). Viral stocks were prepared from the supernatant of infected C6/36 cells, clarified by centrifugation at 800 × *g*, and titrated on Vero cells by a focus-forming assay (FFA). Stocks were kept at −80°C. West Nile virus (WNV) strain IS-98-ST1 (or Stork/98) was obtained, cultured, and used as described by Mashimo et al. (62). Rift Valley fever virus (RVFV) strain ZH548 was obtained, cultured, and used as described by Tokuda et al. (82).

**Mouse experiments.** All infection experiments were performed in a biosafety level 3 animal facility. The mice were maintained in isolators.

**(i) ZIKV and DENV systemic infection.** CC mice received 2 mg of an IFNAR-blocking mouse MAb (MAb MAR1-5A3; BioXCell) by intraperitoneal (i.p.) injection 1 day before ZIKV or DENV infection (83). Groups of 6- to 8-week-old mice were inoculated i.p. with 10<sup>7</sup> focus-forming units (FFUs) of ZIKV FG15 or 10<sup>3</sup> FFUs of ZIKV HD78788 in 200 μl phosphate-buffered saline (PBS). For DENV infection, mice were anesthetized by i.p. injection with a solution of xylazine (5 mg/kg of body weight) and ketamine (80 mg/kg) and afterwards were inoculated by intravenous (i.v.) injection in the retro-orbital sinus with 2 × 10<sup>6</sup> FFUs of DENV-1 KDH0026A in 100 μl PBS. Survival and clinical signs were monitored daily for

up to 14 days. Clinical signs were scored as follows: 0, no symptoms; 1, ruffled fur; 2, emaciation, hunched posture, and/or hypoactivity; 3, hind limb weakness, prostration, and/or closed eyes; and 4, moribund or dead. Blood samples were collected at several time points from the retromandibular vein for plasma viral load assessment.

**(ii) ZIKV intracerebral infection.** Mice were anesthetized by i.p. injection with a solution of xylazine (5 mg/kg), ketamine (75 mg/kg), and buprenorphine (0.03 mg/kg). Groups of 5- to 6-week-old mice were then inoculated by intracerebral (i.c.) injection in the right brain hemisphere with a 26-gauge needle affixed to a Hamilton syringe sheathed by a wire guard allowing no more than a 4-mm penetrance into the skull cavity, as described previously (84). Mice received either  $10^5$  FFUs of ZIKV FG15 in PBS or PBS alone in a volume of 10  $\mu$ l. Survival and clinical signs were monitored daily for 6 days, and the mice were euthanized for brain collection. Another cohort of mice ( $n = 7$  to 8 per strain) was similarly infected and monitored daily for 21 days to assess symptoms and survival.

**(iii) WNV and RVFV infection.** Groups of 8- to 12-week-old mice were inoculated i.p. with  $10^3$  FFUs of WNV strain IS-98-ST1 or  $10^2$  PFU of RVFV strain ZH548. Survival and clinical signs were monitored daily for up to 14 days (RVFV) or 21 days (WNV).

**MEF isolation and infection.** Mouse embryonic fibroblasts (MEFs) were isolated from individual fetuses from one or more genetically identical females at day 13.5 to 14.5 of gestation and cultured in DMEM supplemented with 10% FBS (Eurobio) and 1% penicillin-streptomycin (Gibco) at 37°C. MEFs were used until passage 2.

MEFs were plated at identical densities in culture dishes 24 h before infection. MEFs were infected with the ZIKV FG15 strain at an MOI of 5. After 2 h of incubation at 37°C, the inoculum was replaced with fresh medium. Supernatants were collected at 24, 48, and 72 h p.i. Titration was performed by FFA in Vero cells.

**Focus-forming assay.** Vero cells were seeded at  $3 \times 10^4$  per well in 100  $\mu$ l complete medium (DMEM, 10% FBS) in 96-well plates. After overnight incubation at 37°C, the medium was replaced with 40  $\mu$ l of serial 10-fold dilutions of the samples, and 115  $\mu$ l of methylcellulose overlay was added 2 h later. After 40 h of incubation, the culture medium was removed and cells were fixed with 100  $\mu$ l/well of 4% paraformaldehyde for 20 min and permeabilized with a solution of 0.3% Triton X-100 and 5% FBS in PBS for 20 min. The cells were washed and incubated with a mouse MAbs directed against ZIKV envelop protein (MAb 4G2, purified from the ATCC hybridoma) for 1 h at 37°C (1/250 in blocking buffer). The cells were further washed, incubated with a secondary antibody (Alexa Fluor 488-conjugated anti-mouse IgG; Invitrogen) for 45 min at 37°C, and washed. Infected cell foci were counted using an ImmunoSpot CTL analyzer, and viral titers were calculated from the average number of foci.

**Viral genome quantification by RT-qPCR.** Blood samples were centrifuged to recover plasma from which viral RNA was extracted with a QIAamp viral RNA minikit (Qiagen). Brain tissue samples were homogenized at 4°C in 1 ml of the TRIzol reagent (Life Technologies), using ceramic beads and an automated homogenizer (PreCelllys). Total RNA was extracted according to the manufacturer's instructions. cDNA synthesis was performed using Moloney murine leukemia virus reverse transcriptase (Life Technologies) in a Bio-Rad MyCycler thermocycler. ZIKV and DENV cDNAs were quantified by a TaqMan quantitative PCR (qPCR) in a ViiA7 instrument (Life Technologies), using standard cycling conditions. The following primer sets adapted from previous works (85–87) were used to detect ZIKV and DENV RNA: for ZIKV FG15, forward primer 5'-CCG CTG CCC AAC ACA AG-3' and reverse primer 5'-CCA CTA ACG TTC TTT TGC AGA CAT-3' with the probe 5'-6FAM-AGC CTA CCT TGA CAA GCA ATC AGA CAC TCA A-MGB-3' (Life Technologies) (where 6FAM is 6-carboxyfluorescein); for ZIKV HD78788, forward primer 5'-AAA TAC ACA TAC CAA AAC AAA GTG GT-3' and reverse primer 5'-TCC ACT CCC TCT CTG GTC TTG-3' with the probe 5'-6FAM-CTC AGA CCA GCT GAA G-MGB-3' (Life Technologies); and for DENV-1 KD0026A, forward primer 5'-GGA AGG AGA AGG ACT CCA CA-3' and reverse primer 5'-ATC CTT GTA TCC CAT CCG GCT-3' with the probe 5'-6FAM CTC AGA GAC ATA TCA AAG ATT CCA GGG-MGB-3' (Life Technologies). The viral load is expressed on a  $\log_{10}$  scale as the number of viral genome copies per milliliter (plasma samples) or per number of total RNA micrograms (brain samples) after comparison with a standard curve produced using serial 10-fold dilutions of a plasmid containing the corresponding fragment of ZIKV genome.

**Western blot analysis.** MEFs ( $5 \times 10^6$ ) were preincubated with 100  $\mu$ g IFNAR1-blocking antibody (MAb MARI-5A3; BioXCell) for 7 h and then stimulated or not with 300 IU/ml mouse IFN- $\alpha$  (Miltenyi Biotec) for 15 min. The MEFs were detached and centrifuged at  $300 \times g$  for 5 min, and the cell pellet was resuspended in cold PBS. The MEFs were then lysed into extraction buffer (10 mM Tris-HCl, pH 7.5, 5 mM EDTA, 150 mM NaCl, 1% NP-40, 10% glycerol, 30 mM NaP, 50 mM sodium fluoride), containing protease inhibitor (cOmplete, EDTA free; Roche) and phosphatase inhibitors (phosStop Easy Pack; Roche) in which lysis was completed with 2.5 IU of nuclease (Benzonase; Sigma). The lysates were incubated on ice for 30 min, and the insoluble fraction was separated by centrifugation. Protein concentrations were determined by the Bradford assay, and equal amounts of protein were further used. Protein denaturation was performed in Laemmli buffer at 95°C for 5 min. After separation on a 12% polyacrylamide gel (Bio-Rad), the proteins were transferred on an Immun-Blot polyvinylidene difluoride (PVDF) membrane (Bio-Rad) and incubated overnight with the following antibodies: anti-phospho-STAT1 Tyr701 (1/1,000; catalog number 9167; Cell Signaling), anti-total STAT1 N terminus (1/500; catalog number 610115; BD Biosciences), and anti- $\alpha$ -tubulin (1/8,000; catalog number T5168; Merck). The membranes were incubated for 1.5 h at room temperature with an anti-mouse or an anti-rabbit IgG horseradish peroxidase-linked secondary antibody (1/10,000 MAbs NA931 and NA934V; Amersham), and the signals were visualized using autoradiography.

**Histopathology.** After necropsy, the brain was removed, fixed for 48 to 72 h in 10% neutral buffered formalin, and embedded in paraffin; 4- $\mu$ m-thick sections were stained in hematoxylin-eosin. The morphology of the microglial cells was assessed by immunohistochemistry using rabbit anti-Iba1 primary antibody (1:50 dilution; catalog number 01919741; Wako Chemical) as previously described (88). Sections were analyzed by a trained veterinary pathologist in a study with coded slides carried out in a blind manner. Quantification of the microglia reaction was carried out using automated detection of the Iba1 labeling signal and measurement of the labeled area on a low-magnification ( $\times 2$ ) picture of a brain section of each mouse, using ImageJ software (<https://imagej.nih.gov/ij/>).

**Genetic analysis.** Broad-sense heritability was calculated as previously described (61).

The plasma viral load at days 2 and 6 p.i. and the plasma viral load decrease, measured for 159 mice of the 35 CC strains (average, 4.5 mice per strain), were used in quantitative trait locus (QTL) mapping using the *rqtl2* R package (89) and the GigaMUGA genotypes of the CC founders and CC strains available from <http://csbio.unc.edu/CCstatus/CCGenomes/#genotypes>. A genome scan was performed using the *scan1* function with a linear mixed model using a kinship matrix. Statistical significance levels were calculated from 1,000 permutations.

Genotype-phenotype associations for specific genes (*Ifnar1*, *Oas1b*) were tested by the Kruskal-Wallis test using the founder haplotype as the genotype.

**Statistical analysis.** Statistical analyses were performed using R software (v3.5.2). Kaplan-Meier survival curves were compared by the log-rank test. Two-way ANOVA was used for testing mouse strain and sex effects on the plasma viral load at day 2 p.i. (Fig. 2E). Student's *t* test was used to compare the viral loads in tissues, except when data showed heterogeneous variance between groups, in which case we used Kruskal-Wallis and Wilcoxon nonparametric tests. These tests were also used for assessing the mouse strain effect on the plasma viral load and on the plasma viral load decrease (Fig. 3). Pearson's coefficient was used for determination of the correlation between the plasma viral load at days 2 and 6 p.i. (Fig. 3B) and the correlation between measurements of the plasma viral load determined by FFA and RT-qPCR (Fig. 2D). Student's *t* test was used to compare the viral titers between the strains in *in vitro* experiments. *P* values of  $<0.05$  were considered statistically significant.

## ACKNOWLEDGMENTS

We are grateful to the Virology Laboratory of the Institut Pasteur of French Guiana (National Reference Center for Arboviruses) for providing the FG15 ZIKV strain and Valérie Choumet for providing the IS-98-ST1 WNV strain. We thank Thérèse Couderc and Claude Ruffié for providing B6-*Ifnar1* and 129-*Ifnar1* mice, Laetitia Joullié and Marion Doladilhe for technical help, Magali Tichit for performance of the histopathology techniques, Isabelle Lanctin, Tommy Penel, and Jérôme Le Boydre for careful breeding of the CC mice, and the animal facility staff for animal care in biocontainment units (DTPS-C2RA-Central Animal Facility platform). We are grateful to Jean Jaubert, Michel Cohen-Tannoudji, and Aurore Vidy-Roche for useful discussions throughout the project and to Rachel Meade for editorial suggestions.

We declare no competing interests.

This work was supported by a grant from the French government's Investissement d'Avenir program, Laboratoire d'Excellence Integrative Biology of Emerging Infectious Diseases (grant no. ANR-10-LABX-62-IBEID). C.M. was supported by a fellowship from grant no. ANR-10-LABX-62-IBEID.

## REFERENCES

- Petersen LR, Jamieson DJ, Powers AM, Honein MA. 2016. Zika virus. *N Engl J Med* 374:1552–1563. <https://doi.org/10.1056/NEJMra1602113>.
- Talero-Gutierrez C, Rivera-Molina A, Perez-Pavajeau C, Ossa-Ospina I, Santos-Garcia C, Rojas-Anaya MC, de-la-Torre A. 2018. Zika virus epidemiology: from Uganda to world pandemic, an update. *Epidemiol Infect* 146:673–679. <https://doi.org/10.1017/S0950268818000419>.
- Cao-Lormeau V-M, Blake A, Mons S, Lastère S, Roche C, Vanhomwegen J, Dub T, Baudouin L, Teissier A, Larre P, Vial A-L, Decam C, Choumet V, Halstead SK, Willison HJ, Musset L, Manuguerra J-C, Despres P, Fournier E, Mallet H-P, Musso D, Fontanet A, Neil J, Ghawché F. 2016. Guillain-Barre syndrome outbreak associated with Zika virus infection in French Polynesia: a case-control study. *Lancet* 387:1531–1539. [https://doi.org/10.1016/S0140-6736\(16\)00562-6](https://doi.org/10.1016/S0140-6736(16)00562-6).
- Munoz LS, Parra B, Pardo CA. 2017. Neurological implications of Zika virus infection in adults. *J Infect Dis* 216:S897–S905. <https://doi.org/10.1093/infdis/jix511>.
- Rasmussen SA, Jamieson DJ, Honein MA, Petersen LR. 2016. Zika virus and birth defects—reviewing the evidence for causality. *N Engl J Med* 374:1981–1987. <https://doi.org/10.1056/NEJMsr1604338>.
- Sanz Cortes M, Rivera AM, Yopez M, Guimaraes CV, Diaz Yunes I, Zarutskie A, Davila I, Shetty A, Mahadev A, Serrano SM, Castillo N, Lee W, Valentine G, Belfort M, Parra G, Mohila C, Aagaard K, Parra M. 2018. Clinical assessment and brain findings in a cohort of mothers, fetuses and infants infected with Zika virus. *Am J Obstet Gynecol* 218:440.e1–440.e36. <https://doi.org/10.1016/j.ajog.2018.01.012>.
- Xia H, Luo H, Shan C, Muruato AE, Nunes BT, Medeiros DBA, Zou J, Xie X, Giraldo MI, Vasconcelos PFC, Weaver SC, Wang T, Rajsbaum R, Shi PY. 2018. An evolutionary NS1 mutation enhances Zika virus evasion of host interferon induction. *Nat Commun* 9:414. <https://doi.org/10.1038/s41467-017-02816-2>.
- Liu Y, Liu J, Du S, Shan C, Nie K, Zhang R, Li XF, Zhang R, Wang T, Qin CF, Wang P, Shi PY, Cheng G. 2017. Evolutionary enhancement of Zika virus infectivity in *Aedes aegypti* mosquitoes. *Nature* 545:482–486. <https://doi.org/10.1038/nature22365>.
- Flamand C, Fritzell C, Matheus S, Dueymes M, Carles G, Favre A, Enfissi A, Adde A, Demar M, Kazanji M, Cauchemez S, Rousset D. 2017. The proportion of asymptomatic infections and spectrum of disease among pregnant women infected by Zika virus: systematic monitoring in French

- Guiana, 2016. *Euro Surveill* 22(44):pii=17-00102. <https://doi.org/10.2807/1560-7917.ES.2017.22.44.17-00102>.
10. Cauchemez S, Besnard M, Bompard P, Dub T, Guillemette-Artur P, Eyrolle-Guignot D, Salje H, Van Kerkhove MD, Abadie V, Garel C, Fontanet A, Mallet HP. 2016. Association between Zika virus and microcephaly in French Polynesia, 2013-15: a retrospective study. *Lancet* 387: 2125–2132. [https://doi.org/10.1016/S0140-6736\(16\)00651-6](https://doi.org/10.1016/S0140-6736(16)00651-6).
  11. Brasil P, Pereira JP, Moreira ME, Ribeiro Nogueira RM, Damasceno L, Wakimoto M, Rabello RS, Valderramos SG, Halai U-A, Salles TS, Zin AA, Horovitz D, Daltro P, Boechat M, Raja Gabaglia C, Carvalho de Sequeira P, Pilotto JH, Medialdea-Carrera A, Cotrim da Cunha D, Abreu de Carvalho LM, Pone M, Machado Siqueira A, Calvet GA, Rodrigues Baião AE, Neves ES, Nassar de Carvalho PR, Hasue RH, Marschik PB, Einspieler C, Janzen C, Cherry JD, Bispo de Filippis AM, Nielsen-Saines K. 2016. Zika virus infection in pregnant women in Rio de Janeiro. *N Engl J Med* 375:2321–2334. <https://doi.org/10.1056/NEJMoa1602412>.
  12. McGrath EL, Rossi SL, Gao J, Widen SG, Grant AC, Dunn TJ, Azar SR, Roundy CM, Xiong Y, Prusak DJ, Loucas BD, Wood TG, Yu Y, Fernandez-Salas I, Weaver SC, Vasilakis N, Wu P. 2017. Differential responses of human fetal brain neural stem cells to Zika virus infection. *Stem Cell Rep* 8:715–727. <https://doi.org/10.1016/j.stemcr.2017.01.008>.
  13. Caires-Junior LC, Goulart E, Melo US, Araujo BSH, Alvizi L, Soares-Schanoski A, de Oliveira DF, Kobayashi GS, Griesi-Oliveira C, Musso GM, Amaral MS, daSilva LF, Astray RM, Suarez-Patino SF, Ventini DC, Gomes da Silva S, Yamamoto GL, Equina S, Naslavsky MS, Telles-Silva KA, Weinmann K, van der Linden V, van der Linden H, de Oliveira JMR, Arrais NRM, Melo A, Figueiredo T, Santos S, Meira JCG, Passos SD, de Almeida RP, Bispo AJB, Cavalheiro EA, Kalil J, Cunha-Neto E, Nakaya H, Andreata-Santos R, de Souza Ferreira LC, Verjovski-Almeida S, Ho PL, Passos-Bueno MR, Zatz M. 2018. Discordant congenital Zika syndrome twins show differential in vitro viral susceptibility of neural progenitor cells. *Nat Commun* 9:475. <https://doi.org/10.1038/s41467-017-02790-9>.
  14. Julander JG, Siddharthan V. 2017. Small-animal models of Zika virus. *J Infect Dis* 216:S919–S927. <https://doi.org/10.1093/infdis/jix465>.
  15. Winkler CW, Peterson KE. 2018. Using immunocompromised mice to identify mechanisms of Zika virus transmission and pathogenesis. *Immunology* 153:443–454. <https://doi.org/10.1111/imm.12883>.
  16. Li H, Saucedo-Cuevas L, Regla-Nava JA, Chai G, Sheets N, Tang W, Tersikh AV, Shresta S, Gleeson JG. 2016. Zika virus infects neural progenitors in the adult mouse brain and alters proliferation. *Cell Stem Cell* 19:593–598. <https://doi.org/10.1016/j.stem.2016.08.005>.
  17. Rosenfeld AB, Doobin DJ, Warren AL, Racaniello VR, Vallee RB. 2017. Replication of early and recent Zika virus isolates throughout mouse brain development. *Proc Natl Acad Sci U S A* 114:12273–12278. <https://doi.org/10.1073/pnas.1714624114>.
  18. Tang WW, Young MP, Mamidi A, Regla-Nava JA, Kim K, Shresta S. 2016. A mouse model of Zika virus sexual transmission and vaginal viral replication. *Cell Rep* 17:3091–3098. <https://doi.org/10.1016/j.celrep.2016.11.070>.
  19. Duggal NK, McDonald EM, Ritter JM, Brault AC. 2018. Sexual transmission of Zika virus enhances in utero transmission in a mouse model. *Sci Rep* 8:4510. <https://doi.org/10.1038/s41598-018-22840-6>.
  20. Winkler CW, Woods TA, Rosenke R, Scott DP, Best SM, Peterson KE. 2017. Sexual and vertical transmission of Zika virus in anti-interferon receptor-treated Rag1-deficient mice. *Sci Rep* 7:7176. <https://doi.org/10.1038/s41598-017-07099-7>.
  21. Jaeger AS, Murrieta RA, Goren LR, Crooks CM, Moriarty RV, Weiler AM, Rybarczyk S, Semler MR, Huffman C, Mejia A, Simmons HA, Fritsch M, Osorio JE, Eickhoff JC, O'Connor SL, Ebel GD, Friedrich TC, Aliota MT. 2019. Zika viruses of African and Asian lineages cause fetal harm in a mouse model of vertical transmission. *PLoS Negl Trop Dis* 13:e0007343. <https://doi.org/10.1371/journal.pntd.0007343>.
  22. Yockey LJ, Varela L, Rakib T, Khoury-Hanold W, Fink SL, Stutz B, Szigeti-Buck K, Van den Pol A, Lindenbach BD, Horvath TL, Iwasaki A. 2016. Vaginal exposure to Zika virus during pregnancy leads to fetal brain infection. *Cell* 166:1247–1256.e1244. <https://doi.org/10.1016/j.cell.2016.08.004>.
  23. Miner JJ, Cao B, Govero J, Smith AM, Fernandez E, Cabrera OH, Garber C, Noll M, Klein RS, Noguchi KK, Mysorekar IU, Diamond MS. 2016. Zika virus infection during pregnancy in mice causes placental damage and fetal demise. *Cell* 165:1081–1091. <https://doi.org/10.1016/j.cell.2016.05.008>.
  24. Paul AM, Acharya D, Neupane B, Thompson EA, Gonzalez-Fernandez G, Copeland KM, Garrett M, Liu H, Lopez ME, de Cruz M, Flynt A, Liao J, Guo YL, Gonzalez-Fernandez F, Vig PJS, Bai F. 2018. Congenital Zika virus infection in immunocompetent mice causes postnatal growth impediment and neurobehavioral deficits. *Front Microbiol* 9:2028. <https://doi.org/10.3389/fmicb.2018.02028>.
  25. Caine EA, Jagger BW, Diamond MS. 2018. Animal models of Zika virus infection during pregnancy. *Viruses* 10:E598. <https://doi.org/10.3390/v10110598>.
  26. Wu Y, Liu Q, Zhou J, Xie W, Chen C, Wang Z, Yang H, Cui J. 2017. Zika virus evades interferon-mediated antiviral response through the co-operation of multiple nonstructural proteins in vitro. *Cell Discov* 3:17006. <https://doi.org/10.1038/celldisc.2017.6>.
  27. Pierson TC, Diamond MS. 2018. The emergence of Zika virus and its new clinical syndromes. *Nature* 560:573–581. <https://doi.org/10.1038/s41586-018-0446-y>.
  28. Grant A, Ponia SS, Tripathi S, Balasubramaniam V, Miorin L, Sourisseau M, Schwarz MC, Sánchez-Seco MP, Evans MJ, Best SM, García-Sastre A. 2016. Zika virus targets human STAT2 to inhibit type I interferon signaling. *Cell Host Microbe* 19:882–890. <https://doi.org/10.1016/j.chom.2016.05.009>.
  29. Lazear HM, Govero J, Smith AM, Platt DJ, Fernandez E, Miner JJ, Diamond MS. 2016. A mouse model of Zika virus pathogenesis. *Cell Host Microbe* 19:720–730. <https://doi.org/10.1016/j.chom.2016.03.010>.
  30. Sheehan KC, Lai KS, Dunn GP, Bruce AT, Diamond MS, Heutel JD, Dongo-Arthur C, Carrero JA, White JM, Hertzog PJ, Schreiber RD. 2006. Blocking monoclonal antibodies specific for mouse IFN-alpha/beta receptor subunit 1 (IFNAR-1) from mice immunized by in vivo hydrodynamic transfection. *J Interferon Cytokine Res* 26:804–819. <https://doi.org/10.1089/jir.2006.26.804>.
  31. Smith DR, Hollidge B, Daye S, Zeng X, Blancett C, Kuszpit K, Bocan T, Koehler JW, Coyne S, Minogue T, Kenny T, Chi X, Yim S, Miller L, Schmaljohn C, Bavari S, Golden JW. 2017. Neuropathogenesis of Zika virus in a highly susceptible immunocompetent mouse model after antibody blockade of type I interferon. *PLoS Negl Trop Dis* 11:e0005296. <https://doi.org/10.1371/journal.pntd.0005296>.
  32. Kamiyama N, Soma R, Hidano S, Watanabe K, Umekita H, Fukuda C, Noguchi K, Gendo Y, Ozaki T, Sonoda A, Sachi N, Runtuwene LR, Miura Y, Matsubara E, Tajima S, Takasaki T, Eshita Y, Kobayashi T. 2017. Ribavirin inhibits Zika virus (ZIKV) replication in vitro and suppresses viremia in ZIKV-infected STAT1-deficient mice. *Antiviral Res* 146:1–11. <https://doi.org/10.1016/j.antiviral.2017.08.007>.
  33. Jagger BW, Miner JJ, Cao B, Arora N, Smith AM, Kovacs A, Mysorekar IU, Coyne CB, Diamond MS. 2017. Gestational stage and IFN-lambda signaling regulate ZIKV infection in utero. *Cell Host Microbe* 22:366–376.e363. <https://doi.org/10.1016/j.chom.2017.08.012>.
  34. Tripathi S, Balasubramaniam VRMT, Brown JA, Mena I, Grant A, Bardina SV, Maringer K, Schwarz MC, Maestre AM, Sourisseau M, Albrecht RA, Kramer F, Evans MJ, Fernandez-Sesma A, Lim JK, García-Sastre A. 2017. A novel Zika virus mouse model reveals strain specific differences in virus pathogenesis and host inflammatory immune responses. *PLoS Pathog* 13:e1006258. <https://doi.org/10.1371/journal.ppat.1006258>.
  35. Manet C, Roth C, Tawfik A, Cantaert T, Sakuntabhai A, Montagutelli X. 2018. Host genetic control of mosquito-borne flavivirus infections. *Mamm Genome* 29:384–407. <https://doi.org/10.1007/s00335-018-9775-2>.
  36. Snyder-Keller A, Kramer L, Zink S, Bolivar VJ. 2019. Mouse strain and sex-dependent differences in long-term behavioral abnormalities and neuropathologies after developmental Zika infection. *J Neurosci* 39: 5393–5403. <https://doi.org/10.1523/jneurosci.2666-18.2019>.
  37. Saul MC, Philip VM, Reinholdt LG, Chesler EJ. 2019. High-diversity mouse populations for complex traits. *Trends Genet* 35:501–514. <https://doi.org/10.1016/j.tig.2019.04.003>.
  38. Montagutelli X. 2000. Effect of the genetic background on the phenotype of mouse mutations. *J Am Soc Nephrol* 11(Suppl 16):S101–S105.
  39. Nadeau JH. 2001. Modifier genes in mice and humans. *Nat Rev Genet* 2:165–174. <https://doi.org/10.1038/35056009>.
  40. Collaborative Cross Consortium. 2012. The genome architecture of the Collaborative Cross mouse genetic reference population. *Genetics* 190: 389–401. <https://doi.org/10.1534/genetics.111.132639>.
  41. Roberts A, Pardo-Manuel de Villena F, Wang W, McMillan L, Threadgill DW. 2007. The polymorphism architecture of mouse genetic resources elucidated using genome-wide resequencing data: implications for QTL discovery and systems genetics. *Mamm Genome* 18:473–481. <https://doi.org/10.1007/s00335-007-9045-1>.
  42. Keane TM, Goodstadt L, Danecek P, White MA, Wong K, Yalcin B, Heger A, Agam A, Slater G, Goodson M, Furlotte NA, Eskin E, Nellaker C, Whitley H, Cleak J, Janowitz D, Hernandez-Pliego P, Edwards A, Belgard TG, Oliver PL, McIntyre RE, Bhomra A, Nicod J, Gan X, Yuan W, van der



- Weyden L, Steward CA, Bala S, Stalker J, Mott R, Durbin R, Jackson JJ, Czechanski A, Guerra-Assuncao JA, Donahue LR, Reinholdt LG, Payseur BA, Ponting CP, Birney E, Flint J, Adams DJ. 2011. Mouse genomic variation and its effect on phenotypes and gene regulation. *Nature* 477:289–294. <https://doi.org/10.1038/nature10413>.
43. Rasmussen AL, Okumura A, Ferris MT, Green R, Feldmann F, Kelly SM, Scott DP, Safronetz D, Haddock E, LaCasse R, Thomas MJ, Sova P, Carter VS, Weiss JM, Miller DR, Shaw GD, Korth MJ, Heise MT, Baric RS, de Villena FP, Feldmann H, Katze MG. 2014. Host genetic diversity enables Ebola hemorrhagic fever pathogenesis and resistance. *Science* 346:987–991. <https://doi.org/10.1126/science.1259595>.
  44. Gralinski LE, Ferris MT, Aylor DL, Whitmore AC, Green R, Frieman MB, Deming D, Menachery VD, Miller DR, Buus RJ, Bell TA, Churchill GA, Threadgill DW, Katze MG, McMillan L, Valdar W, Heise MT, Pardo-Manuel de Villena F, Baric RS. 2015. Genome wide identification of SARS-CoV susceptibility loci using the Collaborative Cross. *PLoS Genet* 11: e1005504. <https://doi.org/10.1371/journal.pgen.1005504>.
  45. Graham JB, Thomas S, Swarts J, McMillan AA, Ferris MT, Suthar MS, Treuting PM, Ireton R, Gale M, Jr, Lund JM. 2015. Genetic diversity in the Collaborative Cross model recapitulates human West Nile virus disease outcomes. *mBio* 6:e00493-15. <https://doi.org/10.1128/mBio.00493-15>.
  46. Graham JB, Swarts JL, Wilkins C, Thomas S, Green R, Sekine A, Voss KM, Ireton RC, Mooney M, Choonoo G, Miller DR, Treuting PM, Pardo Manuel de Villena F, Ferris MT, McWeeney S, Gale M, Jr, Lund JM. 2016. A mouse model of chronic West Nile virus disease. *PLoS Pathog* 12:e1005996. <https://doi.org/10.1371/journal.ppat.1005996>.
  47. Green R, Wilkins C, Thomas S, Sekine A, Hendrick DM, Voss K, Ireton RC, Mooney M, Go JT, Choonoo G, Jeng S, de Villena FP, Ferris MT, McWeeney S, Gale M, Jr. 2017. Oas1b-dependent immune transcriptional profiles of West Nile virus infection in the Collaborative Cross. *G3 (Bethesda)* 7:1665–1682. <https://doi.org/10.1534/g3.117.041624>.
  48. Bottomly D, Ferris MT, Aicher LD, Rosenzweig E, Whitmore A, Aylor DL, Haagmans BL, Gralinski LE, Bradel-Tretheway BG, Bryan JT, Threadgill DW, de Villena FP, Baric RS, Katze MG, Heise M, McWeeney SK. 2012. Expression quantitative trait loci for extreme host response to influenza A in pre-collaborative cross mice. *G3 (Bethesda)* 2:213–221. <https://doi.org/10.1534/g3.111.001800>.
  49. Elbahesh H, Schughart K. 2016. Genetically diverse CC-founder mouse strains replicate the human influenza gene expression signature. *Sci Rep* 6:26437. <https://doi.org/10.1038/srep26437>.
  50. Ferris MT, Aylor DL, Bottomly D, Whitmore AC, Aicher LD, Bell TA, Bradel-Tretheway B, Bryan JT, Buus RJ, Gralinski LE, Haagmans BL, McMillan L, Miller DR, Rosenzweig E, Valdar W, Wang J, Churchill GA, Threadgill DW, McWeeney SK, Katze MG, Pardo-Manuel de Villena F, Baric RS, Heise MT. 2013. Modeling host genetic regulation of influenza pathogenesis in the Collaborative Cross. *PLoS Pathog* 9:e1003196. <https://doi.org/10.1371/journal.ppat.1003196>.
  51. Lore NI, Iraqi FA, Bragonzi A. 2015. Host genetic diversity influences the severity of *Pseudomonas aeruginosa* pneumonia in the Collaborative Cross mice. *BMC Genet* 16:106. <https://doi.org/10.1186/s12863-015-0260-6>.
  52. Zhang J, Malo D, Mott R, Panthier JJ, Montagutelli X, Jaubert J. 2018. Identification of new loci involved in the host susceptibility to *Salmonella Typhimurium* in Collaborative Cross mice. *BMC Genomics* 19:303. <https://doi.org/10.1186/s12864-018-4667-0>.
  53. Durrant C, Tayem H, Yalcin B, Cleak J, Goodstadt L, de Villena FP, Mott R, Iraqi FA. 2011. Collaborative Cross mice and their power to map host susceptibility to *Aspergillus fumigatus* infection. *Genome Res* 21: 1239–1248. <https://doi.org/10.1101/gr.118786.110>.
  54. Noll KE, Ferris MT, Heise MT. 2019. The Collaborative Cross: a systems genetics resource for studying host-pathogen interactions. *Cell Host Microbe* 25:484–498. <https://doi.org/10.1016/j.chom.2019.03.009>.
  55. Manet C, Simon-Lorière E, Jouvion G, Hardy D, Prot M, Flamand M, Panthier J-J, Sakuntabhai A, Montagutelli X. 2019. Genetic diversity of Collaborative Cross mice controls viral replication, clinical severity and brain pathology induced by Zika virus infection, independently of *Oas1b*. *bioRxiv* <https://doi.org/10.1101/677484>.
  56. Rossi SL, Tesh RB, Azar SR, Muruato AE, Hanley KA, Auguste AJ, Langsjoen RM, Paessler S, Vasilakis N, Weaver SC. 2016. Characterization of a novel murine model to study Zika virus. *Am J Trop Med Hyg* 94: 1362–1369. <https://doi.org/10.4269/ajtmh.16-0111>.
  57. Dowall SD, Graham VA, Rayner E, Hunter L, Atkinson B, Pearson G, Dennis M, Hewson R. 2017. Lineage-dependent differences in the disease progression of Zika virus infection in type-I interferon receptor knockout (A129) mice. *PLoS Negl Trop Dis* 11:e0005704. <https://doi.org/10.1371/journal.pntd.0005704>.
  58. Srivastava A, Morgan AP, Najarian ML, Sarsani VK, Sigmon JS, Shorter JR, Kashfeen A, McMullan RC, Williams LH, Giusti-Rodriguez P, Ferris MT, Sullivan P, Hock P, Miller DR, Bell TA, McMillan L, Churchill GA, de Villena FP. 2017. Genomes of the mouse Collaborative Cross. *Genetics* 206: 537–556. <https://doi.org/10.1534/genetics.116.198838>.
  59. Scott JM, Lebratti TJ, Richner JM, Jiang X, Fernandez E, Zhao H, Fremont DH, Diamond MS, Shin H. 2018. Cellular and humoral immunity protect against vaginal Zika virus infection in mice. *J Virol* 92:e00038-18. <https://doi.org/10.1128/JVI.00038-18>.
  60. Liang H, Yang R, Liu Z, Li M, Liu H, Jin X. 2018. Recombinant Zika virus envelope protein elicited protective immunity against Zika virus in immunocompetent mice. *PLoS One* 13:e0194860. <https://doi.org/10.1371/journal.pone.0194860>.
  61. Rutledge H, Aylor DL, Carpenter DE, Peck BC, Chines P, Ostrowski LE, Chesler EJ, Churchill GA, de Villena FP, Kelada SN. 2014. Genetic regulation of Zfp30, CXCL1, and neutrophilic inflammation in murine lung. *Genetics* 198:735–745. <https://doi.org/10.1534/genetics.114.168138>.
  62. Mashimo T, Lucas M, Simon-Chazottes D, Frenkiel MP, Montagutelli X, Ceccaldi PE, Deubel V, Guenet JL, Despres P. 2002. A nonsense mutation in the gene encoding 2'-5'-oligoadenylate synthetase/L1 isoform is associated with West Nile virus susceptibility in laboratory mice. *Proc Natl Acad Sci U S A* 99:11311–11316. <https://doi.org/10.1073/pnas.172195399>.
  63. Govero J, Esakky P, Scheaffer SM, Fernandez E, Drury A, Platt DJ, Gorman MJ, Richner JM, Caine EA, Salazar V, Moley KH, Diamond MS. 2016. Zika virus infection damages the testes in mice. *Nature* 540:438–442. <https://doi.org/10.1038/nature20556>.
  64. Manangeeswaran M, Ireland DD, Verthelyi D. 2016. Zika (PRVABC59) infection is associated with T cell infiltration and neurodegeneration in CNS of immunocompetent neonatal C57Bl/6 mice. *PLoS Pathog* 12: e1006004. <https://doi.org/10.1371/journal.ppat.1006004>.
  65. van den Pol AN, Mao G, Yang Y, Ornaghi S, Davis JN. 2017. Zika virus targeting in the developing brain. *J Neurosci* 37:2161–2175. <https://doi.org/10.1523/JNEUROSCI.3124-16.2017>.
  66. Li S, Armstrong N, Zhao H, Hou W, Liu J, Chen C, Wan J, Wang W, Zhong C, Liu C, Zhu H, Xia N, Cheng T, Tang Q. 2018. Zika virus fatally infects wild type neonatal mice and replicates in central nervous system. *Viruses* 10:E49. <https://doi.org/10.3390/v10010049>.
  67. Gorman MJ, Caine EA, Zaitsev K, Begley MC, Weger-Lucarelli J, Uccellini MB, Tripathi S, Morrison J, Yount BL, Dinnon KH, III, Ruckert C, Young MC, Zhu Z, Robertson SJ, McNally KL, Ye J, Cao B, Mysorekar IU, Ebel GD, Baric RS, Best SM, Artyomov MN, Garcia-Sastre A, Diamond MS. 2018. An immunocompetent mouse model of Zika virus infection. *Cell Host Microbe* 23:672–685.e676. <https://doi.org/10.1016/j.chom.2018.04.003>.
  68. Samuel MA, Diamond MS. 2005. Alpha/beta interferon protects against lethal West Nile virus infection by restricting cellular tropism and enhancing neuronal survival. *J Virol* 79:13350–13361. <https://doi.org/10.1128/JVI.79.21.13350-13361.2005>.
  69. Churchill GA, Airey DC, Allayee H, Angel JM, Attie AD, Beatty J, Beavis WD, Belknap JK, Bennett B, Berrettini W, Bleich A, Bogue M, Broman KW, Buck KJ, Buckler E, Burmeister M, Chesler EJ, Cheverud JM, Clapcote S, Cook MN, Cox RD, Crabbe JC, Crusio WE, Darvasi A, Deschepper CF, Doerge RW, Farber CR, Forejt J, Gaile D, Garlow SJ, Geiger H, Gershenfeld H, Gordon T, Gu J, Gu W, de Haan G, Hayes NL, Heller C, Himmelbauer H, Hitzemann R, Hunter K, Hsu HC, Iraqi FA, Ivandic B, Jacob HJ, Jansen RC, Jepsen KJ, Johnson DK, Johnson TE, Kempmann G, et al. 2004. The Collaborative Cross, a community resource for the genetic analysis of complex traits. *Nat Genet* 36:1133–1137. <https://doi.org/10.1038/ng1104-1133>.
  70. Duffy MR, Chen TH, Hancock WT, Powers AM, Kool JL, Lanciotti RS, Pretrick M, Marfel M, Holzbauer S, Dubray C, Guillaumot L, Griggs A, Bel M, Lambert AJ, Laven J, Kosoy O, Panella A, Biggerstaff BJ, Fischer M, Hayes EB. 2009. Zika virus outbreak on Yap Island, Federated States of Micronesia. *N Engl J Med* 360:2536–2543. <https://doi.org/10.1056/NEJMoa0805715>.
  71. Aliota MT, Caine EA, Walker EC, Larkin KE, Camacho E, Osorio JE. 2016. Characterization of lethal Zika virus infection in AG129 mice. *PLoS Negl Trop Dis* 10:e0004682. <https://doi.org/10.1371/journal.pntd.0004682>.
  72. Dowall SD, Graham VA, Rayner E, Atkinson B, Hall G, Watson RJ, Bosworth A, Bonney LC, Kitchen S, Hewson R. 2016. A susceptible mouse model for Zika virus infection. *PLoS Negl Trop Dis* 10:e0004658. <https://doi.org/10.1371/journal.pntd.0004658>.

73. do Valle TZ, Billecocq A, Guillemot L, Alberts R, Gommet C, Geffers R, Calabrese K, Schughart K, Bouloy M, Montagutelli X, Panthier JJ. 2010. A new mouse model reveals a critical role for host innate immunity in resistance to Rift Valley fever. *J Immunol* 185:6146–6156. <https://doi.org/10.4049/jimmunol.1000949>.
74. Le-Trilling VT, Trilling M. 2017. Mouse newborn cells allow highly productive mouse cytomegalovirus replication, constituting a novel convenient primary cell culture system. *PLoS One* 12:e0174695. <https://doi.org/10.1371/journal.pone.0174695>.
75. Setoh YX, Peng NY, Nakayama E, Amarilla AA, Prow NA, Suhrbier A, Khromykh AA. 2018. Fetal brain infection is not a unique characteristic of Brazilian Zika viruses. *Viruses* 10:541. <https://doi.org/10.3390/v10100541>.
76. Savidis G, Perreira JM, Portmann JM, Meraner P, Guo Z, Green S, Brass AL. 2016. The IFITMs inhibit Zika virus replication. *Cell Rep* 15:2323–2330. <https://doi.org/10.1016/j.celrep.2016.05.074>.
77. Horisberger MA, Staeheli P, Haller O. 1983. Interferon induces a unique protein in mouse cells bearing a gene for resistance to influenza virus. *Proc Natl Acad Sci U S A* 80:1910–1914. <https://doi.org/10.1073/pnas.80.7.1910>.
78. Keele GR, Crouse WL, Kelada SNP, Valdar W. 2019. Determinants of QTL mapping power in the realized Collaborative Cross. *G3 (Bethesda)* 9:1707–1727. <https://doi.org/10.1534/g3.119.400194>.
79. Simon-Loriere E, Lin RJ, Kalayanarooj SM, Chuansumrit A, Casademont I, Lin SY, Yu HP, Lert-Itthiporn W, Chaiyaratana W, Tangthawornchaikul N, Tangnaratchakit K, Vasanawathana S, Chang BL, Suriyaphol P, Yoksan S, Malasit P, Despres P, Paul R, Lin YL, Sakuntabhai A. 2015. High anti-dengue virus activity of the OAS gene family is associated with increased severity of dengue. *J Infect Dis* 212:2011–2020. <https://doi.org/10.1093/infdis/jiv321>.
80. Welsh CE, Miller DR, Manly KF, Wang J, McMillan L, Morahan G, Mott R, Iraqi FA, Threadgill DW, de Villena FP. 2012. Status and access to the Collaborative Cross population. *Mamm Genome* 23:706–712. <https://doi.org/10.1007/s00335-012-9410-6>.
81. Fansiri T, Fontaine A, Diancourt L, Caro V, Thaisomboonsuk B, Richardson JH, Jarman RG, Ponlawat A, Lambrechts L. 2013. Genetic mapping of specific interactions between *Aedes aegypti* mosquitoes and dengue viruses. *PLoS Genet* 9:e1003621. <https://doi.org/10.1371/journal.pgen.1003621>.
82. Tokuda S, Do Valle TZ, Batista L, Simon-Chazottes D, Guillemot L, Bouloy M, Flamand M, Montagutelli X, Panthier JJ. 2015. The genetic basis for susceptibility to Rift Valley fever disease in MBT/Pas mice. *Genes Immun* 16:206–212. <https://doi.org/10.1038/gene.2014.79>.
83. Sheehan KC, Lazear HM, Diamond MS, Schreiber RD. 2015. Selective blockade of interferon-alpha and -beta reveals their non-redundant functions in a mouse model of West Nile virus infection. *PLoS One* 10:e0128636. <https://doi.org/10.1371/journal.pone.0128636>.
84. Shimizu S. 2004. Chapter 32. Routes of administration, p 527–542. *In* Hedrich HJ, Bullock G (ed), *The laboratory mouse*. Academic Press, London, United Kingdom. <https://doi.org/10.1016/B978-012336425-8/50085-6>.
85. Lanciotti RS, Kosoy OL, Laven JJ, Velez JO, Lambert AJ, Johnson AJ, Stanfield SM, Duffy MR. 2008. Genetic and serologic properties of Zika virus associated with an epidemic, Yap State, Micronesia, 2007. *Emerg Infect Dis* 14:1232–1239. <https://doi.org/10.3201/eid1408.080287>.
86. Faye O, Faye O, Diallo D, Diallo M, Weidmann M, Sall AA. 2013. Quantitative real-time PCR detection of Zika virus and evaluation with field-caught mosquitoes. *Virology* 10:311. <https://doi.org/10.1186/1743-422X-10-311>.
87. Fontaine A, Jiolle D, Moltini-Conclois I, Lequime S, Lambrechts L. 2016. Excretion of dengue virus RNA by *Aedes aegypti* allows non-destructive monitoring of viral dissemination in individual mosquitoes. *Sci Rep* 6:24885. <https://doi.org/10.1038/srep24885>.
88. Verdonk F, Roux P, Flamant P, Fiette L, Bozza FA, Simard S, Lemaire M, Plaud B, Shorte SL, Sharshar T, Chretien F, Danckaert A. 2016. Phenotypic clustering: a novel method for microglial morphology analysis. *J Neuroinflammation* 13:153. <https://doi.org/10.1186/s12974-016-0614-7>.
89. Broman KW, Gatti DM, Simecek P, Furlotte NA, Prins P, Sen S, Yandell BS, Churchill GA. 2019. R/qtl2: software for mapping quantitative trait loci with high-dimensional data and multiparent populations. *Genetics* 211:495–502. <https://doi.org/10.1534/genetics.118.301595>.